

# RXTE all-sky slew survey. Catalog of X-ray sources at $|b| > 10^\circ$

M. Revnivtsev<sup>1,2</sup>, S. Sazonov<sup>1,2</sup>, K. Jahoda<sup>3</sup>, M. Gilfanov<sup>1,2</sup>

<sup>1</sup> Max-Planck-Institut für Astrophysik, Karl-Schwarzschild-Str. 1, D-85740 Garching bei München, Germany

<sup>2</sup> Space Research Institute, Russian Academy of Sciences, Profsoyuznaya 84/32, 117997 Moscow, Russia

<sup>3</sup> Laboratory for High Energy Astrophysics, Code 662, Goddard Space Flight Center, Greenbelt, MD 20771, USA

**Abstract.** We report results of a serendipitous hard X-ray (3–20 keV), nearly all-sky ( $|b| > 10^\circ$ ) survey based on RXTE/PCA observations performed during satellite reorientations in 1996–2002. The survey is 80% (90%) complete to a  $4\sigma$  limiting flux of  $\approx 1.8$  ( $2.5$ )  $\times 10^{-11}$  erg s $^{-1}$  cm $^{-2}$  in the 3–20 keV band. The achieved sensitivity in the 3–8 keV and 8–20 keV subbands is similar to and an order of magnitude higher than that of the previously record HEAO-1 A1 and HEAO-1 A4 all-sky surveys, respectively. A combined  $7 \times 10^3$  sq. deg area of the sky is sampled to flux levels below  $10^{-11}$  erg s $^{-1}$  cm $^{-2}$  (3–20 keV). In total 294 sources are detected and localized to better than 1 deg. 236 (80%) of these can be confidently associated with a known astrophysical object; another 22 likely result from the superposition of 2 or 3 closely located known sources. 35 detected sources remain unidentified, although for 12 of these we report a likely soft X-ray counterpart from the ROSAT all-sky survey bright source catalog. Of the reliably identified sources, 63 have local origin (Milky Way, LMC or SMC), 64 are clusters of galaxies and 100 are active galactic nuclei (AGN). The fact that the unidentified X-ray sources have hard spectra suggests that the majority of them are AGN, including highly obscured ones ( $N_{\mathrm{H}} > 10^{23}$  cm $^{-2}$ ). For the first time we present a log  $N$ -log  $S$  diagram for extragalactic sources above  $4 \times 10^{-12}$  erg s $^{-1}$  cm $^{-2}$  at 8–20 keV.

**Key words.** cosmology:observations – diffuse radiation – X-rays:general

## 1. Introduction

The deep surveys performed recently in the standard X-ray band (2–10 keV) with the Chandra and XMM-Newton observatories (e.g. Brandt et al. 2001, Hasinger et al. 2001) have convincingly proved the extragalactic origin of the cosmic X-ray background (CXB). Hundreds of point sources detected in these surveys provide us with a wealth of information about the distant Universe. However, due to the very small sky coverage of these surveys, they are practically unsuitable for the study of the local Universe ( $z \lesssim 0.3$ ). Medium-sensitivity ( $10^{-13}$ – $10^{-12}$  erg cm $^{-2}$  s $^{-1}$ ) X-ray surveys, such as those performed with ASCA (Ueda et al. 1999) and BeppoSAX (Giommi et al. 2000), cover larger areas of the sky ( $\lesssim 10^2$  sq. deg) but also cannot sample efficiently the Universe within  $\sim 500$  Mpc of us. In this regard, the results of the soft X-ray ( $< 2$  keV) all-sky survey carried out with the ROSAT observatory (e.g. Voges et al. 1999) are extremely important, but these cannot be directly extrapolated into the  $> 2$  keV energy band. Therefore, our knowledge of the statistical properties of the local population of hard X-ray sources still rests largely on the snapshot of the whole sky taken in the 2–100 keV energy band more than 20 years ago by the different experiments on

board the HEAO-1 observatory, A1 (Wood et al. 1984), A2 (Piccinotti et al. 1982) and A4 (Levine et al. 1984). It is only now that we have the possibility to undertake a new hard X-ray (3–20 keV) all-sky survey at similar (below 10 keV) and much better (above 10 keV) sensitivity provided by the RXTE observatory.

The Rossi X-ray Timing Explorer (RXTE, Bradt et al. 1993) was launched at the end of 1995 and has now been successfully operating for more than 7 years. The mission was primarily designed to study the variability of X-ray sources on time scales from sub-milliseconds to years (e.g. Swank et al. 1995). The maneuvering capability of the satellite combined with the high photon throughput of its main detector (PCA) has also made it possible to carry out a series of Galactic Bulge scans aimed at the detection of new transient sources and following the long-term behavior of known X-ray sources (Markwardt et al. 2000). In addition, over its still continuing life time, RXTE/PCA has collected a large amount of data of slew observations covering almost the entire sky. In the current work we use these data to perform an all-sky survey in the 3–20 keV energy band. The relatively narrow field of view of the PCA instrument allows us to localize sources to better than 1 deg and thus effectively avoid source confusion after we restrict our consideration to Galactic latitudes  $|b| > 10^\circ$ .

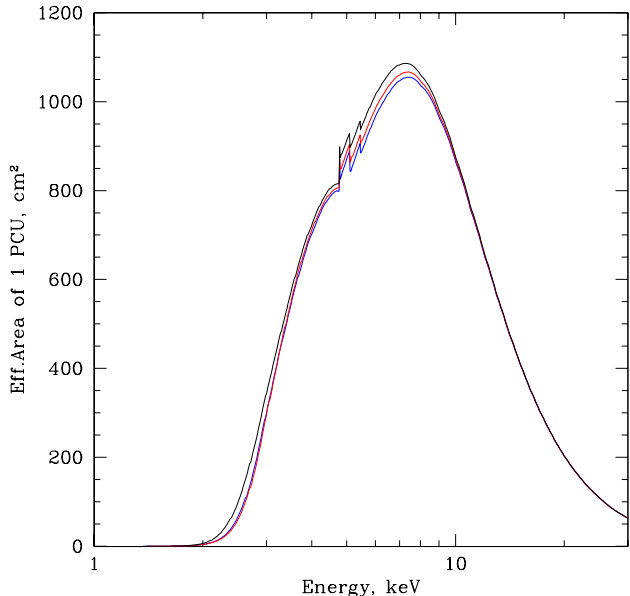


**Fig. 1.** Effect of high voltage variations on the PCU effective area. Shown is the effective area of PCU2 on Apr. 17, 1996 (epoch 3), Dec. 06, 1999 (epoch 4) and June 15, 2002 (epoch 5)

We note that the RXTE/PCA slew data have previously been utilized to reconstruct the average spectrum of the CXB (Revnivtsev et al. 2003).

## 2. Data analysis

### 2.1. Data selection and reduction

One of the main instruments aboard the RXTE observatory is the Proportional Counter Array (PCA), an X-ray spectrometer. It consists of 5 nearly identical Proportional Counter Units (PCUs). Each PCU is sensitive to photons with energies 2–60 keV, reaching the maximum effective area at  $\sim 7$  keV. For an X-ray source with a Crab-like spectrum, most of the counts would be detected at energies below 10 keV. However, a significant effective area,  $300$ – $500$   $\text{cm}^2$  per PCU, is also available in the 10–20 keV energy band.

The slewing rate of the RXTE satellite between targets is  $<0.1$   $\text{deg s}^{-1}$ . One can make use of data collected during such reorientations to build maps of the sky. We have utilized the slew parts of all RXTE observations performed from April 15, 1996–July 16, 2002. This amounts in total to approximately 50,000 observations of typical length 200–500 s. The observational period before April 15, 1996 (High Voltage Epochs 1 and 2) was excluded from the analysis because during that time the PCA had significantly different gain and dependence of the effective area on energy. Since these early observations constitute

only  $\sim 2.5\%$  of all available slew/scan data, their rejection has negligible effect on the net exposure time of our survey, which is 20.2 Ms.

The data reduction was done using standard tools of the LHEASOFT/FTOOLS 5.2 package. In this version of the software the effective area of the PCA detectors is slightly ( $\sim 11$ – $12\%$ ) underestimated, which leads to an overestimation of the fluxes of X-ray sources (see Revnivtsev et al. 2003, Jahoda et al. 2004, in preparation). We have made a correction for this factor in our analysis.

For the background modeling we used the faint source ("L7\_240") CM model (<http://heasarc.gsfc.nasa.gov/docs/xte/recipes/pcabackest.html>). The background model includes by design both the CXB and instrumental background. Therefore, the background subtracted rate for "blank sky" observations is expected to be consistent with zero within spacial fluctuations of the CXB. The rms amplitude of these fluctuations (cosmic variance) was earlier estimated for RXTE/PCA to be  $\sim 7\%$ , or  $\sim 1.5 \times 10^{-12}$   $\text{erg s}^{-1} \text{cm}^{-2}$ , in the 2–10 keV energy band (Markwardt et al. 2002, Revnivtsev et al. 2003).

At low galactic latitude, there is diffuse X-ray emission from the Galactic ridge and bulge. Using results of Iwan et al. 1982 and Revnivtsev 2003, we estimate that this component does not exceed  $\sim 2$ – $3 \times 10^{-12}$   $\text{ergs s}^{-1} \text{cm}^{-2}$  at  $|b| > 10^\circ$  in the central part of the Galaxy and continues to decrease with distance from the Galactic center (in  $l$  and  $b$ ). We therefore neglect the Galactic diffuse emission in our subsequent analysis.

In order to reduce the effect of the uncertainties in the PCA background subtraction and increase our sensitivity to source detection, we used only the data of the first layer (LR1) for all PCUs. The effective area of a PCU (the first upper anode layer only) is shown as a function of photon energy in Fig. 1. Different curves in the figure represent different high voltage epochs of the PCA. The observed variations of the effective area prove to be mainly due to an increasing amount of xenon in the propane layer (Jahoda et al. 2004, in preparation) rather than due to the change of the high voltage.

We utilized data of Standard2 mode of the PCA, which are available for all observations. Standard2 mode provides the possibility of energy band selection and also 16 s time resolution. Energy band selection is very important, because by using a band narrower than the PCA total energy range (2–60 keV) we can significantly reduce the instrumental background and therefore strongly increase our sensitivity to faint sources. However, during a 16-s interval the center of the PCA field of view can move up to  $1$ – $1.5^\circ$ , which limits the spatial resolution of maps constructed from Standard2 data (see §2.3 for further discussion of this issue).

Data were filtered by the following criteria. We filtered out Earth occulted data (by applying the criterion  $ELV > 10$ ). Our study of the PCA background subtraction uncertainties and their dependence on the

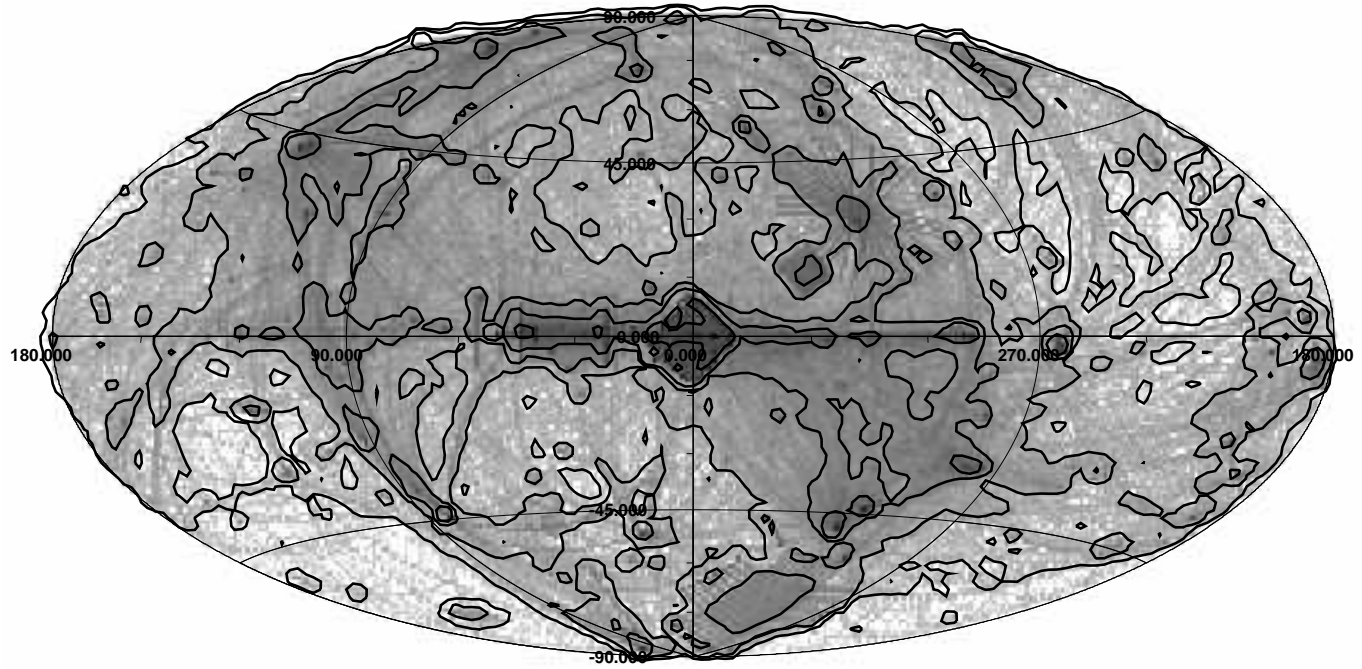


**Fig. 2.** Sky exposure map (in Galactic coordinates) of the RXTE/PCA slew survey performed during April 1996–July 2002, recalculated per one PCU area. Smoothed contours are drawn at 100, 300, 1000, 3000, 10000 and  $30000 \text{ s deg}^{-2}$ .

*ELECTRON* rate demonstrated that for our purposes (weak source detection) it is better to use the criterion  $ELECTRON\_PCU0, 1, 2, 3, 4 < 0.085$  than the standard condition  $< 0.1$ . In addition, we excluded all data from PCU0 obtained later than May 12, 2000, because the loss of the upper propane veto layer of this PCU has resulted in strongly increased background subtraction uncertainties. After applying the above filters we are left with 9.3 Ms exposure time worth of good data, covering almost all of the sky. Since during some slews not all 5 PCUs were operational, the resulting exposure time recalculated per one PCU is 26.9 Ms. The corresponding exposure map is shown in Fig. 2.

## 2.2. Sensitivity and completeness of the survey

To avoid dealing with substantial source confusion due to high density of Galactic X-ray sources, we excluded observations performed at low Galactic latitude  $|b| < 10^\circ$  from the construction of a catalog of detected sources (see §3). The total accumulated exposure time per PCU corresponding to the  $|b| > 10^\circ$  region (with the total area of 34,090 sq. deg) is 16.6 Ms.

Fig. 3 shows the effective survey area as a function of the minimum PCU count rate allowing  $4\sigma$  source detection in the 3–20 keV, 3–8 keV and 8–20 keV bands, and also as a function of an energy flux threshold for  $4\sigma$  detection of sources with a Crab-like spectrum (power law with a photon index  $\Gamma = 2$ ). The survey is 80%

(90%) complete at  $|b| > 10^\circ$  down to 3–20 keV, 3–8 keV and 8–20 keV count rates of 1.8 (2.5), 1.2 (1.6) and 1.3 (1.8)  $\text{cnt s}^{-1}$ . For  $\Gamma = 2$  sources, these numbers correspond to the following limiting fluxes: 2.3 (3.3), 1.2 (1.6) and  $2.5 (3.4) \times 10^{-11} \text{ erg s}^{-1} \text{ cm}^{-2}$ . The sensitivity of the RXTE slew survey below 10 keV is thus comparable to/slightly higher than that of the HEAO-1 A1/A2 surveys (Wood et al. 1984, Piccinotti et al. 1982). In the 10–20 keV energy band, the current slew survey has record sensitivity for all-sky hard X-ray surveys, being an order of magnitude deeper than the HEAO-1/A4 survey (Levine et al. 1984).

## 2.3. Construction of the all-sky map; detection and localization of sources

Relatively fast and irregular slews of the RXTE satellite do not allow us to detect weak sources using the procedures previously applied to the analysis of the UHURU and HEAO-1 all-sky surveys (Forman et al. 1978, Piccinotti et al. 1982, Wood et al. 1984). For this reason, our source detection algorithm is based on analyzing averaged maps of the sky instead of using individual scans.

The accuracy of source localization depends on the source brightness and variability as well as on the RXTE slewing speed, but is always better than  $1 - 1.5^\circ$  for a single slew across a source. The localization of a source that has been scanned across several times can be signif-

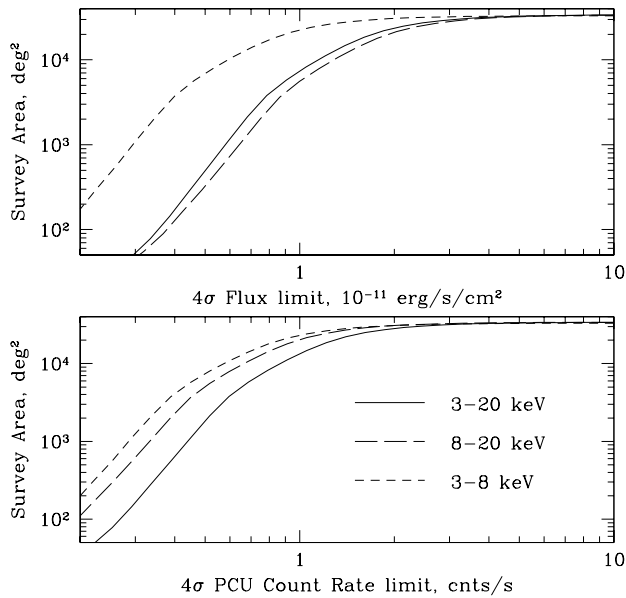


**Fig. 3.** Sky coverage at  $|b| > 10^\circ$  of the RXTE/PCA slew survey as a function of the minimum count rate (lower panel) and energy flux (assuming a Crab-like source spectrum, upper panel) needed for detection of a source at  $4\sigma$  confidence level in different energy bands.

icantly improved by fitting its observed brightness profile on the sky with a model of the collimator response. The locations of extremely stable and strong sources such as the Crab nebula or brightest clusters of galaxies can thus be recovered within few arcminutes.

A sequence of several steps, as described below, was performed to build the all-sky map and to detect and localize sources in the sky. First, a map of the sky for each PCU was obtained by ascribing the measured, background subtracted count rate to the celestial position toward which the center of the PCA field of view was pointed at the middle of each 16-s bin of data. Such maps were produced in the total 3–20 keV energy band as well as in the subbands 3–8 keV and 8–20 keV. Then, exposure-weighted averaging of the maps from the individual PCUs was done to obtain raw maps of the sky in the three energy bands.

The derived all-sky maps are of very high statistical quality as demonstrated in Fig. 4, where we present the distribution of the observed signal-to-noise ( $S/N$ )<sup>1</sup>) ratios for the  $\sim 34,000 1^\circ \times 1^\circ$  bins making up the sky map at  $|b| > 10^\circ$  in the 3–20 keV band. The chosen pixel size assures that neighbouring bins are practically independent, because the effective field of view of RXTE/PCA is 1 sq.

<sup>1</sup> Here  $N$  means purely statistical noise of the measurements. We do not include here the variations of the CXB brightness level, which are smaller than the statistical uncertainty of a source flux measurement for typical exposure times  $\sim 100$  s

deg. In the case of pure statistical noise, the  $S/N$  distribution is expected to be a Gaussian with zero mean and unity dispersion, which is quite similar to what is actually observed for  $S/N < 2$  (see Fig. 4). Given this excellent agreement, we require that a source have a  $S/N > 4$  in the 3–20 keV band to be considered detected. With this criterion, we allow the detection of approximately one fake source over the whole sky at  $|b| > 10^\circ$ .

A simply binned raw map of the sky does not provide us with the best signal to noise ratio for the search of point sources. In order to maximally use the available statistics we convolved the raw all-sky maps with the response of the RXTE/PCA collimator (Jahoda et al. 1996). The resulting 3–20 keV all-sky map is shown in Fig. 5. This map was used to detect sources by searching for peaks characterized by a  $S/N$  ratio of more than 4. The positions and fluxes of so found sources were subsequently determined from a  $\chi^2$  fit of the PCA collimator model to the raw all-sky map. In our catalog of detected sources (see §3), their best-fit positions are given with a  $1\sigma$  statistical uncertainty.

However, the above procedure is not optimal for detection and localization of sources covered by only a few RXTE slews and for strongly variable sources. We therefore also searched the  $1^\circ$ -binned raw all-sky map for pixels that have  $S/N > 4$ . This has allowed us to detect several additional sources, missed in the previous step (convolved sky analysis). For these sources, a conservative estimate of the total localization uncertainty is provided in the catalog (see §3). In all cases, the error is less than or equal to  $1^\circ$ .

#### 2.4. Flux measurement and source confusion

Measurement of source fluxes in our survey is subject to some systematic uncertainties. Some uncertainty may arise from insufficiently accurate determination of source positions. The further the inferred position is from the actual one, the smaller flux can be ascribed to the source because of the response of the collimator falling off with increasing offset from the optical axis. This should not however result in a biased estimate of the flux of a source that has been covered by numerous slews, because in that case both the source position and its flux are determined simultaneously from a fit of the model collimator response to the source image. However, the effect may be important for poorly covered sources and also for variable and transient sources. As most of the sky in our survey is covered by more than 5 slews, the effect is expected to be generally small.

We could estimate the accuracy of the flux determination if we had a sample of persistent sources with known X-ray fluxes. Fortunately, there are 64 clusters of galaxies detected in our survey (see §3) for most of which we can compare their measured RXTE/PCA 3–8 keV count rates with the corresponding values evaluated from the fluxes and gas temperatures derived

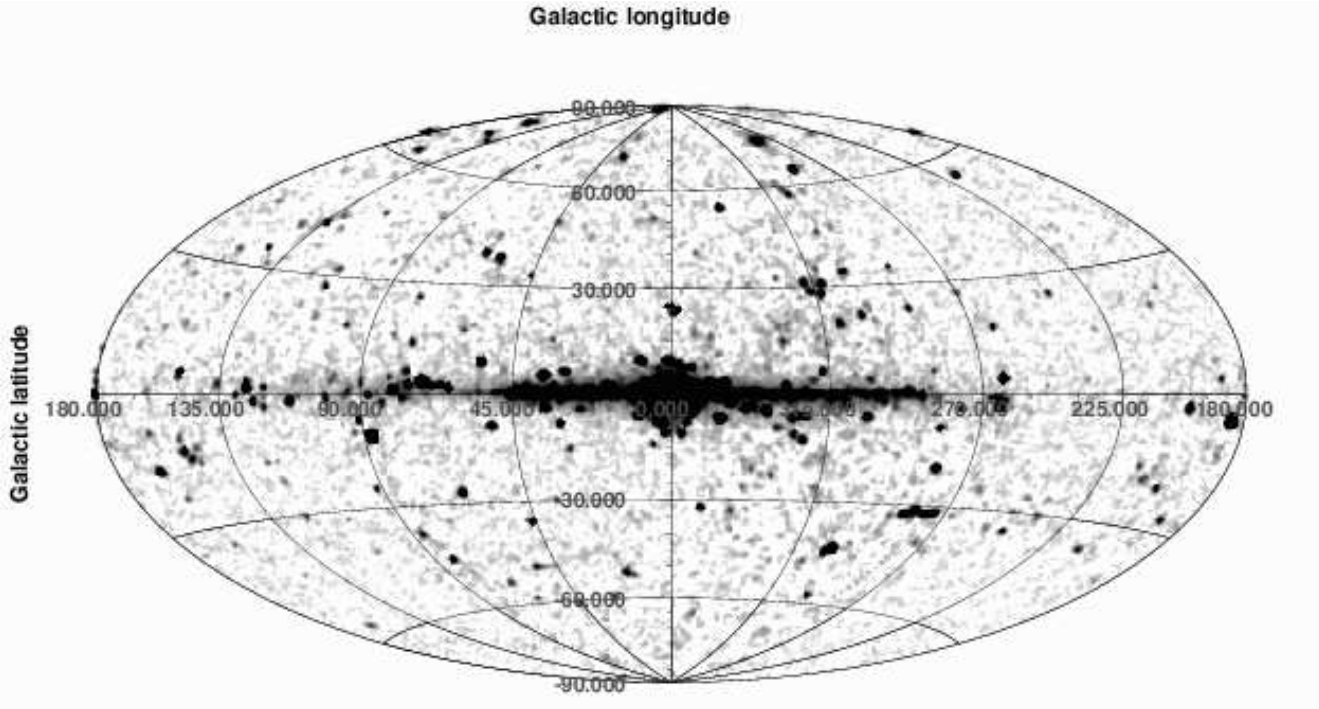


**Fig. 5.** All-sky map obtained with RXTE/PCA in the 3–20 keV energy band

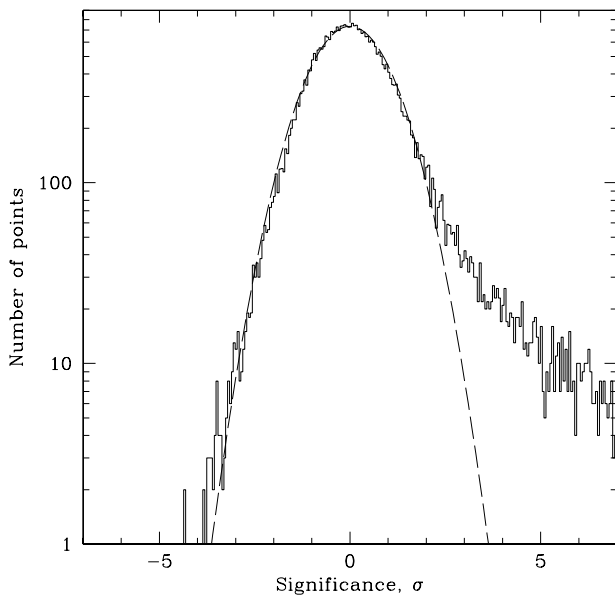


**Fig. 4.** Distribution of signal-to-noise ratios for  $\sim 34,000$   $1^\circ \times 1^\circ$  bins making up the  $|b| > 10^\circ$  sky map in the 3–20 keV band. The dashed line is a Gaussian with zero mean and unity dispersion, expected for pure statistical noise.

with ROSAT and ASCA observatories (Markevitch 1998, Ebeling et al. 2000, Ikebe et al. 2002). The fact that clus-

ters of galaxies are not point sources does not strongly affect our flux estimates because of the low ( $\sim 1^\circ$ ) angular resolution of our measurements. The strongest deviations from the true source flux, on the order of 20–30%, may arise in the case of largest clusters of galaxies such as the Coma.

It can be seen from Fig. 6 that the agreement between the two sets of count rates is very good and there seems to be no significant bias in our flux determination even for angular offsets as large as  $40'$ . Since for the absolute majority of sources in our catalog that can be confidently associated with a known astrophysical object the RXTE location is within  $40'$  of the true position, we will not attempt to correct any of the measured fluxes for the possible bias described above. We note however that the fluxes of the (weak and poorly localized) unidentified sources in our catalog may be systematically underestimated.

Because of the fairly large field of view of the PCA ( $\sim 1$  sq. deg), source confusion presents some problem for our survey. Confusion may manifest itself through the appearance of two or more sufficiently bright sources within our beam and lead to ambiguous source identification and uncertainty in source flux determination. Using cumulative source counts interpolated from HEAO-1/A2, ASCA and BeppoSAX measurements, or the consistent estimate from the current survey (see §4.2), and taking into account the sky coverage and sensitivity of our survey (Fig. 3), we may estimate that there can be of the order of 10 unresolvable pairs and larger groups of sources, detectable as single sources with  $S/N > 4$ , on the sky at  $|b| > 10^\circ$ , assuming a uniform distribution of sources. We do find a

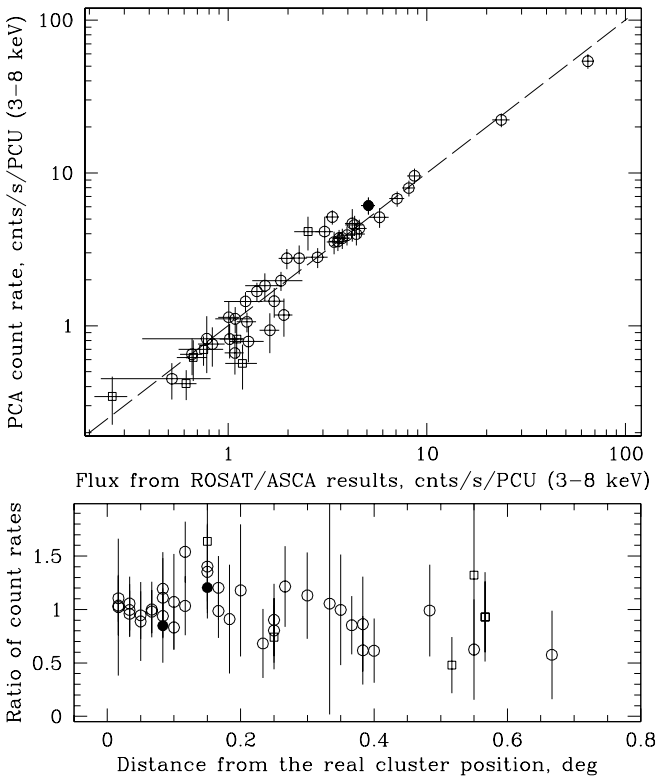


**Fig. 6. Upper panel:** Count rates measured in the RXTE/PCA slew survey vs. count rates predicted from fluxes and gas temperatures measured with ROSAT and ASCA for 45 clusters of galaxies. The data are taken from Ikebe et al. (2002) – open circles, Markevitch (1998) – solid circles, and Ebeling et al. (2000) – open squares. **Lower panel:** Ratio of the measured and predicted count rates as a function of distance of the localization from the true position of clusters.

comparable number of confusion cases (groups of known X-ray sources) in our catalog (see §3).

The uncertainty of the flux determination can be expressed in terms of confusion variance  $\sigma_{\text{conf}}$ . In the case of a power-law form of cumulative source counts (the number of sources with a flux greater than  $f$  per unit solid angle),  $N(> f) = Cf^{-\alpha}$ , the confusion noise is given by

$$f/\sigma_{\text{conf}}(f) = \left( \frac{\alpha}{2 - \alpha} \Omega N(> f) \right)^{-1/2},$$

where  $\Omega$  is the effective solid angle of the instrument beam (e.g. Hacking & Houck 1987). For the standard value  $\alpha = 1.5$  and the observed density of sources, we find that confusion sets in at count rates below  $4\sigma_{\text{conf}} \approx 0.5 \text{ cnt s}^{-1}$  in the 3–20 keV band, or equivalently (assuming a Crab-like spectrum) at fluxes below  $7 \times 10^{-12} \text{ erg s cm}^{-2}$ .

Summarizing the above discussion, we can conclude that our estimates of source fluxes may be affected by confusion in the count rate range below  $0.5 \text{ cnt s}^{-1}$ , or for fluxes below  $7 \times 10^{-12} \text{ erg s cm}^{-2}$  (over 3–20 keV), and therefore  $\sim 20$  of sources entering the catalog at these levels should be treated with caution.

### 3. The catalog

A total of 294 sources detected (with higher than  $4\sigma$  significance) in the 3–20 keV energy band at Galactic latitudes  $|b| > 10^\circ$  comprise the RXTE slew survey catalog, which is presented in Table 2. The columns of the catalog are described below.

*Column (1)* – source entry name in the catalog. “XSS” stands for “XTE Slew Survey”. The name provides the source equatorial coordinates (2000).

*Columns (2,3)* – source Galactic coordinates.

*Column (4)* – localization region radius. In cases where the standard procedure of fitting the collimator response to the source brightness profile is unreliable, a conservative estimate of the total localization uncertainty is given. Otherwise, the quoted value represents  $1\sigma$  statistical uncertainty.

*Columns (5,6)* – count rate and  $1\sigma$  statistical uncertainty (in  $\text{cnt s}^{-1}$  per PCU) for the 3–8 keV energy band.

*Columns (7,8)* – count rate and  $1\sigma$  statistical uncertainty (in  $\text{cnt s}^{-1}$  per PCU) for the 8–20 keV energy band.

*Column (9,10)* – effective slope (photon index) of the source spectrum and  $1\sigma$  uncertainty. This estimate is based on the ratio of the 8–20 keV and 3–8 keV count rates. A lower (upper) limit is given in cases where the upper (lower) band flux measurement has a signal-to-noise ratio of less than 2.

*Column (11)* – common name of astrophysical object with which the XSS source is identified. There may be several entries per XSS source. The identification procedure is described in §3.1.

*Columns (12)* – general astrophysical type of the associated object. L – local (source in the Milky Way, LMC or SMC), A – active galactic nucleus, C – cluster of galaxies, G – non-active galaxy, O – other – afterglow of a gamma-ray burst.

*Columns (13)* – more detailed classification of object. For AGN (A): Q – quasar, RQQ – radio-quite quasar, RLQ – radio-loud quasar, BL – blasar (BL Lac object or flat-spectrum radio quasar), S1 – Seyfert 1 galaxy (types 1, 1.2 and 1.5), NLS1 – narrow-line Seyfert 1 galaxy, S2 – Seyfert 2 galaxy (types 1.8, 1.9 and 2), RG – radio galaxy, BLRG – broad-line radio galaxy, NLRG – narrow-line radio galaxy, LLAGN – low luminosity AGN. AGN classification is mostly adopted from NED, otherwise references are provided. For “local” sources (L): XB – X-ray binary, P – polar, IP – intermediate polar, DN – dwarf nova of SU, UG or ZC type, NL – nova-like of VY type, S – hot star, RS CVn – RS CVn variable star, SS – symbiotic star.

*Columns (14)* – redshift (if known) for extragalactic sources.

*Columns (15)* – additional notes or references.

Table 1 provides a set of conversion coefficients allowing one to estimate the flux of a cataloged source in the 3–8 keV, 8–20 keV and 3–20 keV bands in units of  $\text{erg s}^{-1} \text{ cm}^{-2}$  from the count rates given in the catalog for a number of values of the effective spectral slope.

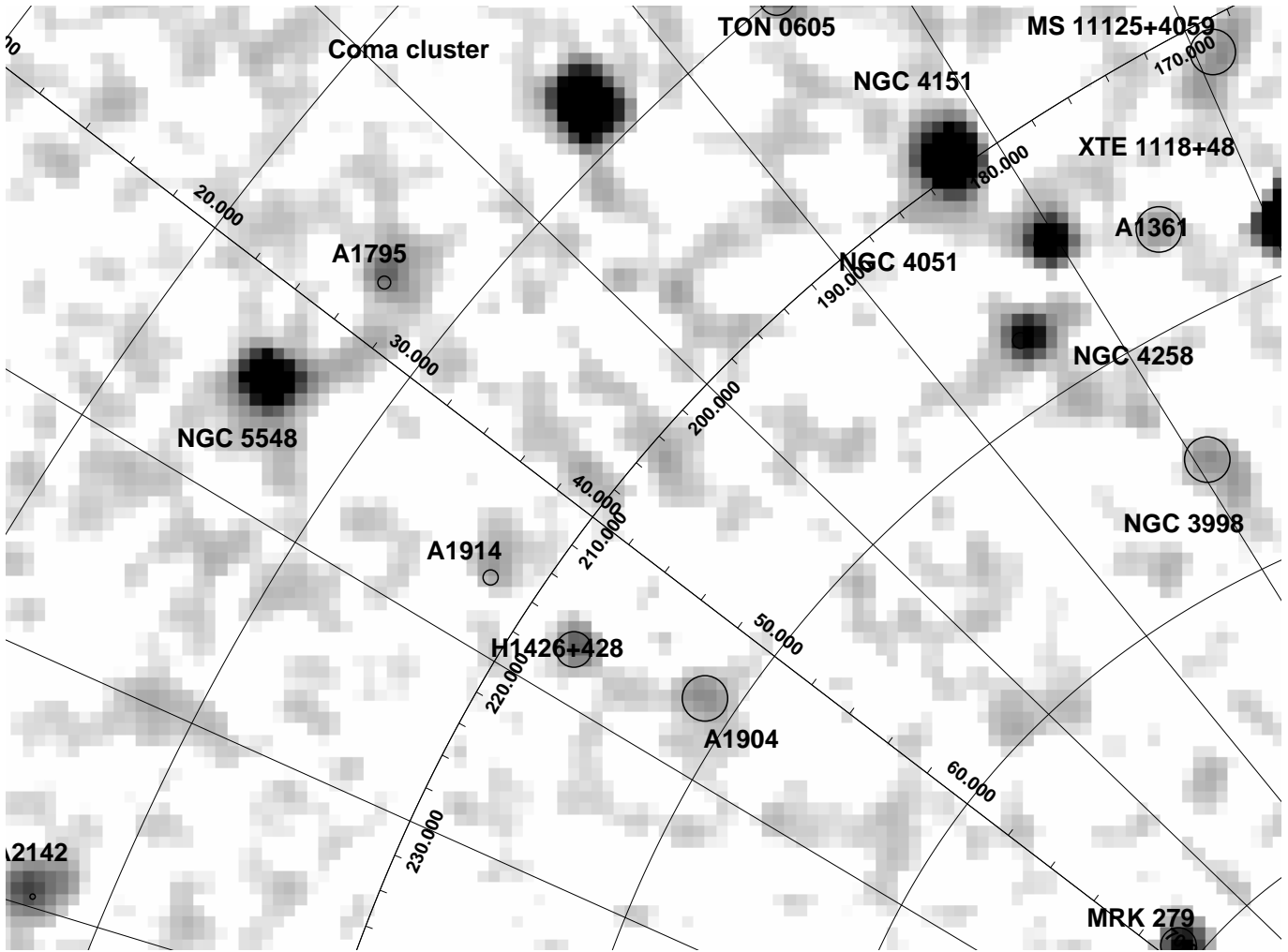


**Fig. 7.** Map of the sky around  $l=80^\circ$ ,  $b=70^\circ$  in the energy band 3-20 keV. The gray scale represents the significance of the detection of X-ray flux from a location in the sky. Circles (very small in the case of bright sources such as Coma cluster) and labels denote uncertainty radii of detected sources and their likely identifications, respectively.

**Table 1.** Conversion factor ( $A$ ) between the RXTE/PCA count rates ( $CR$ ) and the source energy flux ( $F$ ) as a function of the source spectral slope ( $\Gamma$ ):  $F (10^{-11} \text{ erg s}^{-1} \text{ cm}^{-2}) = A \times CR (\text{cnt s}^{-1})$ .

	-1	-0.5	0	1	2	3
3-8 keV	0.67	0.88	1.00	1.04	1.03	1.02
8-20 keV	2.71	2.89	2.87	2.45	1.92	1.51
3-20 keV	2.29	2.39	2.27	1.75	1.33	1.12

### 3.1. Identification of sources

We have searched for likely counterparts to the hard X-ray sources detected in our survey primarily making use of large astronomical databases including NED, SIMBAD and VizieR. The identification process was greatly facilitated thanks to the availability of the ROSAT all-sky survey bright source catalog (RBSC, Voges et al. 1999) of soft X-ray (0.1-2.4 keV) sources. The ROSAT survey is typically an order of magnitude more sensitive than our RXTE slew survey for sources with Crab-like spectra

( $\Gamma \sim 2$ ). Therefore, in most cases we could unambiguously associate the XSS source with a single bright (typically  $\gtrsim 0.2 \text{ cnt s}^{-1}$ ) and hard (typically  $HR1 > 0.5$ ) RBSC source located within the RXTE error box. Furthermore, for most of such highly probable associations the astrophysical type is known and other related information (such as redshift) is available, and that is included in the catalog. In addition, the ASCA Medium Sensitivity Survey (the GIS catalog, Ueda et al. 2001) played a crucial role in deciding about the identification of a number of sources.

In those cases where we strongly believe that the XSS source is associated with a particular RBSC source but its nature remains unknown, we just quote the ROSAT name in the identification column. In addition, among the sources of unknown nature in our catalog there are 6 whose localizations are consistent with a HEAO-1/A1 source (Wood et al. 1984). Such associations are also indicated in the catalog.

Very hard sources in our catalog such as Seyfert 2 galaxies may have no obvious counterpart in the RBSC catalog, and even in the ROSAT all-sky survey faint

source catalog, due to a low-energy photoabsorption cut-off in their X-ray spectrum. We thus carefully browsed published samples of AGN, in particular Seyfert 2s, observed by focusing X-ray telescopes operating in the standard 2–10 keV band (TARTARUS/ASCA database, Bassani et al. 1999), searching for possible associations with our sources.

In addition, we have identified 14 XSS sources (including 3 confused cases) located in the so-called Zone of Avoidance at  $10^\circ < |b| < 20^\circ$  with clusters of galaxies recently discovered in the CIZA survey (Ebeling et al. 2002, Ebeling et al. 2004).

For completeness, we included in the catalog four sources associated with gamma-ray burst afterglows. These detections have become possible only due to the RXTE observatory targeting these afterglows and therefore represent an extremely biased statistics of the occurrence of GRB X-ray afterglows on the sky. The effect of cataloged sources being RXTE targets on the statistics of the catalog is discussed below.

### 3.2. Effect of RXTE pointing at cataloged sources

149 out of the 294 detected sources in our catalog were at least once the target of RXTE/PCA pointed observations. Although we have not used the data of the pointed observations themselves, the slew parts of these observations were included in our analysis. One may therefore reasonably suspect that some sources have entered the catalog only because they had been chosen for observations with RXTE.

In order to check this hypothesis we have re-evaluated the significance of detection of all cataloged sources by excluding the data of the slews associated with pointing at the sources. It turns out that apart from the GRB afterglows only the sources Mrk 335, Mrk 348, Ton S180 and NGC 1068 (all are AGN) would not have qualified for a catalog entry if they had not been pointed at by RXTE. Since this affects only  $\sim 1\%$  of the catalog, we conclude that the effect of targeting on the statistical quality of the catalog is negligible.

## 4. Analysis of the catalog

Out of the 294 detected sources, 236 (80%) have been associated with a single known astrophysical object, another 22 probably result from superposition of 2 or 3 closely located known sources. 35 detected sources remain unidentified, although for 12 of these there is a probable soft X-ray counterpart from the RBSC. Of the reliably identified single sources, 63 have local origin (among them are 19 X-ray binaries, 7 polars and 12 intermediate polars), 64 are clusters of galaxies and 100 are AGN.

### 4.1. Unidentified sources

The astrophysical origin of 35 sources in our catalog remains unknown. For 5 of these detections, the measured 3-

20 keV count rate falls below our adopted confusion limit of 0.5  $\text{cnt s}^{-1}$  (see §2.4), so some of them may in fact result from superposition of weaker sources. 29 unidentified sources are newly discovered hard X-ray sources, while the remaining 6 positionally coincide with previously known HEAO-1 sources (Wood et al. 1984). It should be relatively straightforward to identify in other bands of the electromagnetic spectrum the 12 XSS sources that have a likely RBSC counterpart, because the positions of these sources are known to within 1 arcmin. However, the identification of the other sources can be more problematic. We note that the current localization error ( $\sim 30'$ ) can be significantly reduced by performing slowly scanning RXTE observations of the sources.

We could get some idea as to the nature of the unidentified sources by comparing their effective spectral slopes with those of the XSS sources of known type. This is done in Fig. 8, where we show the distribution of values of the effective photon index for XSS sources divided into several major classes, including AGN, clusters of galaxies, magnetic cataclysmic variables (CVs, including polars and intermediate polars) and unidentified sources. In plotting these diagrams, each source was ascribed a distribution of hardness ratios (8–20 keV/3–8 keV) in accordance with the measured count rate uncertainties.

The resulting distribution of  $\Gamma$  values is apparently broad for the sample of unidentified sources, although substantial part of this scatter results from the statistical uncertainty in measuring the count rates. However, the bulk of the unidentified sources are evidently harder than typical clusters of galaxies, being similar in hardness ( $\Gamma \lesssim 2$ ) to AGN and magnetic CVs.

It is interesting that 31 of 35 unidentified sources are located in the southern hemisphere (at  $\delta < 0$ ), which probably reflects the fact that the southern sky is relatively less studied in the optical and other bands. We can use this fact to show that magnetic CVs are unlikely to constitute the majority of our unidentified sources. Indeed, 8 and 11 of the magnetic CVs in our catalog are located at  $\delta > 0$  and  $\delta < 0$ , respectively. Since these objects are located in space within  $\sim 500$  pc from us, their distribution in the sky is expected to be random to a first approximation. This statement relies on the fact that for a given source luminosity our survey samples similar volumes in the northern and southern hemispheres (in 1 to 1.1 proportion). For comparison, the catalog of CVs by Ritter et al. 2003, which contains 107 polars and intermediate polars and among them all of our 19 magnetic CVs, does not demonstrate any significant north/south asymmetry either: 49 and 58 sources are located at  $\delta > 0$  and  $\delta < 0$ , respectively. If many of our unidentified sources were magnetic CVs, the distribution of all detected sources of this type would become significantly asymmetric with respect to the equatorial plane, which would be very difficult to explain.

Our catalog also includes 44 local sources of types other than magnetic CVs. However, we do not expect that more than a few objects of these types may be present

among our unidentified sources. Indeed, X-ray binaries are very rare and bright X-ray sources, while the other sources (such as hot stars) are also rare and usually have soft spectra ( $\Gamma > 2$ ), as evidenced by our catalog.

We conclude that most of the unidentified sources are likely AGN, including those absorbed at soft X-rays (such as Seyfert 2 galaxies). The AGN content of the RXTE/PCA all-sky slew survey will be discussed in detail in a separate paper.

#### 4.2. Number-flux functions

The high completeness ( $\sim 90\%$ ) of the identification of detected sources allows us to estimate number-flux functions for extragalactic sources. Furthermore, thanks to the record sensitivity achieved by the current survey at 8–20 keV, we obtain a unique opportunity to construct a  $\log N - \log S$  distribution in this hard X-ray band.

Fig. 9 shows the cumulative flux distributions of the detected extragalactic sources in the 2–10 keV and 8–20 keV energy bands, estimated as follows. We selected from the general catalog (Table 2) two samples of sources 1) those having  $S/N > 4$  in the 3–8 keV band and 2) those meeting the same condition in the 8–20 keV band. Excluding sources of confirmed local origin, we are left with 209 and 92 sources for the soft and hard bands, respectively. These samples include unidentified sources (27 and 7, respectively), although the results remain essentially unchanged if we exclude these cases from consideration (8 unidentified sources have  $S/N < 4$  in the soft energy band and 28 sources – in the hard energy band). As was explained in §2.3, although the general catalog comprises sources originally detected in the broad 3–20 keV band, the source samples subsequently selected from it in the 3–8 keV and 8–20 keV subbands are expected to be highly complete.

The  $\log N - \log S$  curves were calculated using the known sky coverage as a function of the survey sensitivity in the 3–8 keV and 8–20 keV bands (Fig. 3). The obtained distributions were converted from count rates to flux units assuming a power-law spectrum of  $\Gamma = 2$ . In addition, to facilitate comparison of our results with those of previous experiments we have made a change from the 3–8 keV band used in the catalog to the standard 2–10 keV band. Finally, we truncated the  $\log N - \log S$  distributions at the lowest fluxes according to the confusion limit formulated in §2.4, namely at  $6 \times 10^{-12}$  erg s cm $^{-2}$  and  $4 \times 10^{-12}$  erg s cm $^{-2}$  in the 2–10 keV and 8–20 keV, respectively. These values result from the fits to the number-flux functions at higher fluxes, presented below. As a result, the final flux distributions for the soft and hard bands presented in Fig. 9 are based on 197 and 90 sources, respectively.

Assuming the usual power-law form for the number-flux function

$$N(> S) = K S^{-\alpha},$$

we can estimate the parameters of this function using the maximum likelihood method (e.g. Crawford, Jauncey & Murdoch 1970). We obtain the following best fits to the observed distributions in the flux ranges  $6 \times 10^{-12} - 6 \times 10^{-10}$  erg s cm $^{-2}$  (3–8 keV) and  $4 \times 10^{-12} - 4 \times 10^{-10}$  erg s cm $^{-2}$  (8–20 keV):

$$N(> S_{11}) = (9 \pm 1) \times 10^{-3} S_{11}^{-1.34 \pm 0.13} \text{ deg}^{-2} \text{ (2 - 10 keV)}$$

and

$$N(> S_{11}) = (5.8 \pm 0.6) \times 10^{-3} S_{11}^{-1.52 \pm 0.18} \text{ deg}^{-2} \text{ (8 - 20 keV)},$$

where  $S_{11}$  is the source flux in units of  $10^{-11}$  erg s $^{-1}$  cm $^{-2}$ , the uncertainties here and later being  $1\sigma$ .

If we fix the slope of the number-flux function at the value  $\alpha = 1.5$ , we obtain normalization constants  $K = (1.0 \pm 0.1) \times 10^{-2}$  and  $K = (5.6 \pm 0.6) \times 10^{-3}$  deg $^{-2}$  for the soft and hard energy bands, respectively.

It is interesting to compare the above normalization of the 2–10 keV cumulative source counts with the values inferred from previous sky surveys, carried out with Ariel 5 (Warwick & Pye 1978), UHURU (Forman et al. 1978), HEAO-1/A2 (Piccinotti et al. 1982) and BeppoSAX (Giommi et al. 2000). Adopting conversion factors of 1 cnt s $^{-1}$  (Ariel 5) =  $6.2 \times 10^{-11}$  erg s $^{-1}$  cm $^{-2}$ , 1 cnt s $^{-1}$  (UHURU) =  $2.4 \times 10^{-11}$  erg s $^{-1}$  cm $^{-2}$  and 1 cnt s $^{-1}$  (HEAO-1/A2) =  $2.4 \times 10^{-11}$  erg s $^{-1}$  cm $^{-2}$  for the 2–10 keV energy band, we find the following coefficients (in the units given above) of the cumulative distribution function:  $K_{\text{Ariel 5}} = (1.5 \pm 0.4) \times 10^{-2}$ ,  $K_{\text{UHURU}} = (1.8 \pm 0.2) \times 10^{-2}$ ,  $N_{\text{HEAO-1/A2}} = (1.24 \pm 0.14) \times 10^{-2}$ ,  $K_{\text{BeppoSAX}} = 8.9 \times 10^{-3}$ .

It can be seen that the Ariel 5, UHURU and HEAO-1 normalizations are slightly higher than ours. This difference probably results from the fact that our estimate of the density of extragalactic sources is largely based on low flux ( $\lesssim 2 \times 10^{-11}$  erg s $^{-1}$  cm $^{-2}$ ) sources that were inaccessible to those experiments. Our result is therefore less affected by the substantially inhomogeneous distribution of X-ray sources in the local extragalactic cell ( $\lesssim 100$  Mpc in size), because we efficiently sample the local Universe outside this volume as well. We note that the source counts measured with RXTE at flux levels above a few  $\times 10^{-11}$  erg s $^{-1}$  cm $^{-2}$ , where the contribution of the local density inhomogeneity becomes important, lie above our power-law fit and are in fact consistent with the results of the early all-sky surveys mentioned above. On the other hand, the extrapolation of our  $\log N - \log S$  curve to fluxes below the limit of the current survey of  $6 \times 10^{-12}$  erg s $^{-1}$  cm $^{-2}$  (2–10 keV) is in excellent agreement with the flux distributions derived from the BeppoSAX and ASCA medium-sensitivity surveys (see Fig. 9).

#### 4.3. Summary

We presented the serendipitous hard X-ray (3–20 keV) survey of the sky at high Galactic latitude  $|b| > 10^\circ$  based on RXTE/PCA slew observations in 1996–2002.

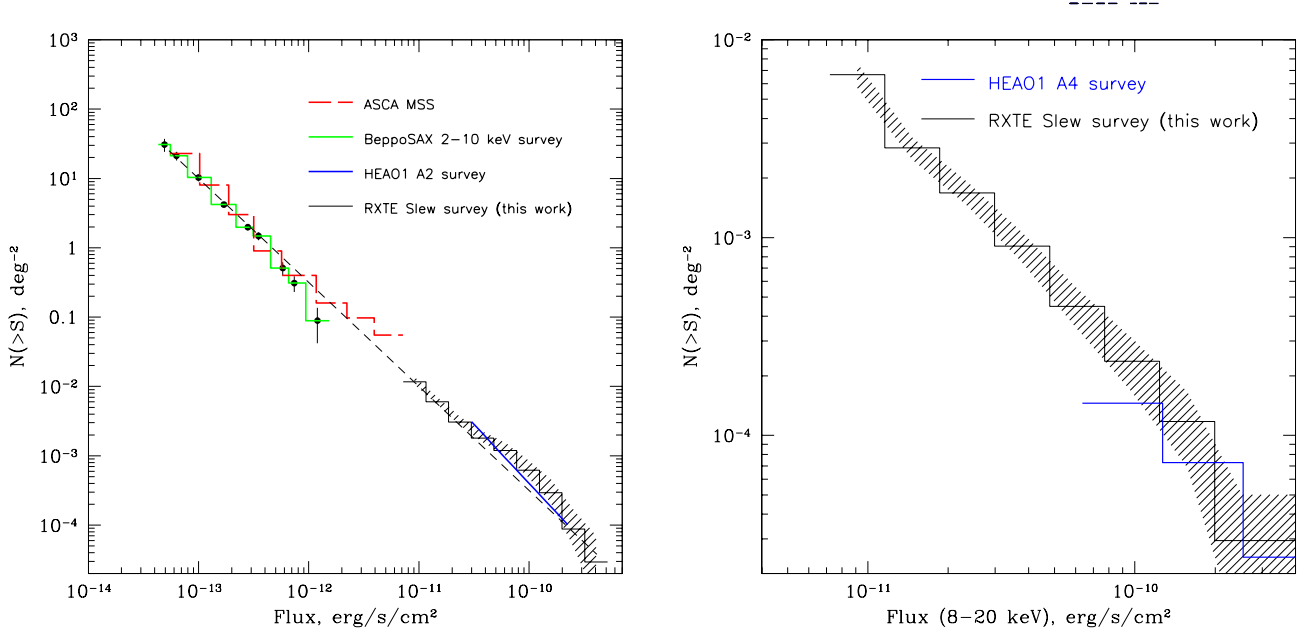


**Fig. 9. Left:** Cumulative log  $N - \log S$  function in the 2–10 keV band obtained from the RXTE all-sky slew survey. To obtain this plot, the count rates measured at 3–8 keV were converted to 2–10 keV fluxes assuming a power law spectrum with a photon index  $\Gamma = 2$ . The dashed area represents the estimated statistical uncertainty. Also shown are a number of previous measurements with: HEAO-1/A2 (Piccinotti et al. 1982), ASCA (Ueda et al. 1999) and BeppoSAX (Giommi et al. 2000). The short-dashed line is our best fit with the slope  $\alpha = 1.5$  to the RXTE data extrapolated down to the fluxes sampled by the BeppoSAX and ASCA surveys. **Right:** Cumulative log  $N - \log S$  function in the 8–20 keV band obtained from the RXTE slew survey. Also shown is the result of the HEAO-1/A4 experiment (Levine et al. 1984) recalculated from the 13–25 keV band to 8–20 keV assuming a  $\Gamma = 2$  spectrum.

At photon energies above 10 keV, the current survey surpasses by an order of magnitude in depth the previously best HEAO-1/A4 survey, achieving similar sensitivity ( $\sim 2 \times 10^{-11} \text{ erg s}^{-1} \text{ cm}^{-2}$ ) to the HEAO-1/A1 experiment in the standard X-ray band (2–10 keV) for the most of the sky. At the same time,  $\sim 20\%$  of the sky is now covered at flux levels below  $10^{-11} \text{ erg s}^{-1} \text{ cm}^{-2}$  (2–10 keV), which has allowed us to draw the  $\log N - \log S$  diagram for extragalactic X-ray sources down to  $6 \times 10^{-12} \text{ erg s}^{-1} \text{ cm}^{-2}$  and thus to fill the previously existing gap toward the cumulative source counts measured at lower fluxes by medium sensitivity surveys. Moreover, we have for the first time estimated the distribution of source fluxes at 8–20 keV in the  $4 \times 10^{-12}$ – $4 \times 10^{-10} \text{ erg s}^{-1} \text{ cm}^{-2}$  range.

The compiled catalog comprises 294 detected sources and provides for each of them the estimated flux and effective spectral slope in the 3–20 keV range. The identification of the sources is already highly complete (88%), so the catalog can be efficiently used for statistical studies of different classes of sources. However, particularly interesting scientific content might still be hidden in the sample of 35 unidentified sources. A large fraction of these are probably AGN, including a number of highly obscured ones which are very difficult to discover in the optical or soft X-ray

bands. To establish their origin, a dedicated identification program needs to be carried out. Scanning RXTE observations could improve the localizations of those unidentified sources for which we failed to find a counterpart in the ROSAT all-sky survey.

The statistical properties of the AGN detected in the RXTE all-sky slew survey will be discussed in a separate paper (Sazonov et al., in preparation).

*Acknowledgements.* We thank Harald Ebeling and Christopher Mullis for providing us the information about a set of CIZA clusters before publication. This research has made use of data obtained through the High Energy Astrophysics Science Archive Research Center Online Service, provided by the NASA/Goddard Space Flight Center.

## References

- Alcalá, J.M., Krautter, J., Schmitt, J.H.M.M. et al. 1995, A&AS, 114, 109
- Bassani, L. et al. 1999, ApJS, 121, 473
- Bradt, H.V., Rotshild R.E., & Swank J.H. 1993, A&AS, 97, 355
- Brandt, W.N. et al., 2001, AJ, 122, 2810
- Brinkmann, W., Siebert, J., Feigelson, E.D., et al. 1997, A&A, 323, 739

Crawford, D.F., Jauncey, D.L., & Murdoch, H.S. 1970, *ApJ*, 162, 405

della Ceca, R., Palumbo, G.G.C., Persic, M. et al. 1990, *ApJS*, 72, 471

Ebeling, H., Edge, A.C., Allen, S.W., Crawford, C.S., Fabian, A.C., & Huchra, J.P. 2000, *MNRAS*, 318, 333

Ebeling, H., Mullis, C.R., & Tully, R.B. 2002, *ApJ*, 580, 774

Ebeling, H. et al., 2004, in preparation

Fischer, J.-U., Hasinger, G., Schwone, A.D. et al. 1998, *Astron. Nachr.*, 319, 347

Forman, W., Jones, C., Cominsky, L. et al., 1978, *ApJS*, 38, 357

Giommi, P., Perri, M., & Fiore, F., 2000, *A&A*, 362, 799

Hacking, P., & Houck, J.R., 1987, *ApJS*, 63, 311

Hasinger, G. et al., 2001, *A&A*, 365, L45

Ikebe, Y., Reiprich, T. H., Böhringer, H., Tanaka Y., & Kitayama, T., 2002, *A&A*, 383, 773

Imanishi, K., Koyama, K., & Tsuboi, Y. 2001, *ApJ*, 557, 747

Iwan D., Marshall F., Boldt E. et al. 1982, *ApJ*, 260, 111

Jahoda, K., Swank, J.H., Giles, A.B., Stark, M.J., Strohmayer, T., Zhang, W., & Morgan, E.H., 1996, *Proc SPIE*, 2808, 59

Lara, L., Márquez, I., Cotton, W.D. et al., 1999, *NewAR*, 43, 643

Laurent-Muehleisen, S.A., Kollgaard, R.I., Ryan, P.J., et al. 1997, *A&AS*, 122, 235

Levine, A.M., Lang, F.L., Lewin, W.H.G. et al. 1984, *ApJS*, 54, 581

Markevitch, M., 1998, *ApJ*, 504, 27

Markwardt, C., Swank, J., Marshall, F., & in't Zand, J., 2000, in ROSSI 2000: Astrophysics with the Rossi X-ray Timing Explorer. March 22-24, 2000 at NASA's GSFC, Greenbelt, MD USA, p. E7

Markwardt, C., Jahoda, K. & Smith, D.A., 2002, <http://lheawww.gsfc.nasa.gov/users/craigm/pca-bkg/bkg-users.html>

Pellegrini, S., Cappi, M., Bassani, L., della Ceca, R., & Palumbo, G.G.C. 2000, *A&A*, 360, 878

Piccinotti, G., Mushotzky, R.F., Boldt, E.A. et al., 1982, *ApJ*, 253, 485

Revnivtsev M. 2003, *A&A*, 410, 865

Revnivtsev, M., Gilfanov, M., Sunyaev, R., Jahoda, K., & Markwardt, C., 2003, *A&A*, 411, 329

Schmid, H.M., Appenzeller, I., & Burch, U., 2003, *A&A*, 404, 505

Simpson, C., Ward, M., Clements, D.L., & Rawlings, S. 1996, *MNRAS*, 281, 509

Swank, J. et al., 1995, The Lives of Neutron Stars, eds. Alpar, A., Kizilolu, U., & van Paradijs, J. NATO ASI Series

Ueda, Y., Takahashi, T., Ishisaki, Y., Ohashi, T., & Makishima, K. 1999, *ApJ*, 524, L11

Ueda, Y., Ishisaki, Y., Takahashi, T., Makishima, K., & Ohashi, T. 2001, *ApJS*, 133, 1

Véron-Cetty, M.-P., Véron, P., & Gonçalves, A.C. 2001, *A&A*, 372, 730

Véron-Cetty, M.-P., & Véron, P. 2003, *A&A*, 412, 399

Voges, W., Aschenbach, B., Boller, Th. et al., 1999, *A&A*, 349, 389

Warwick, R.S., & Pye, J.P., 1978, *MNRAS*, 183, 169

Wood, K.S., Meekins, J.F., Yentis, D.J. et al. 1984, *ApJS*, 56, 507

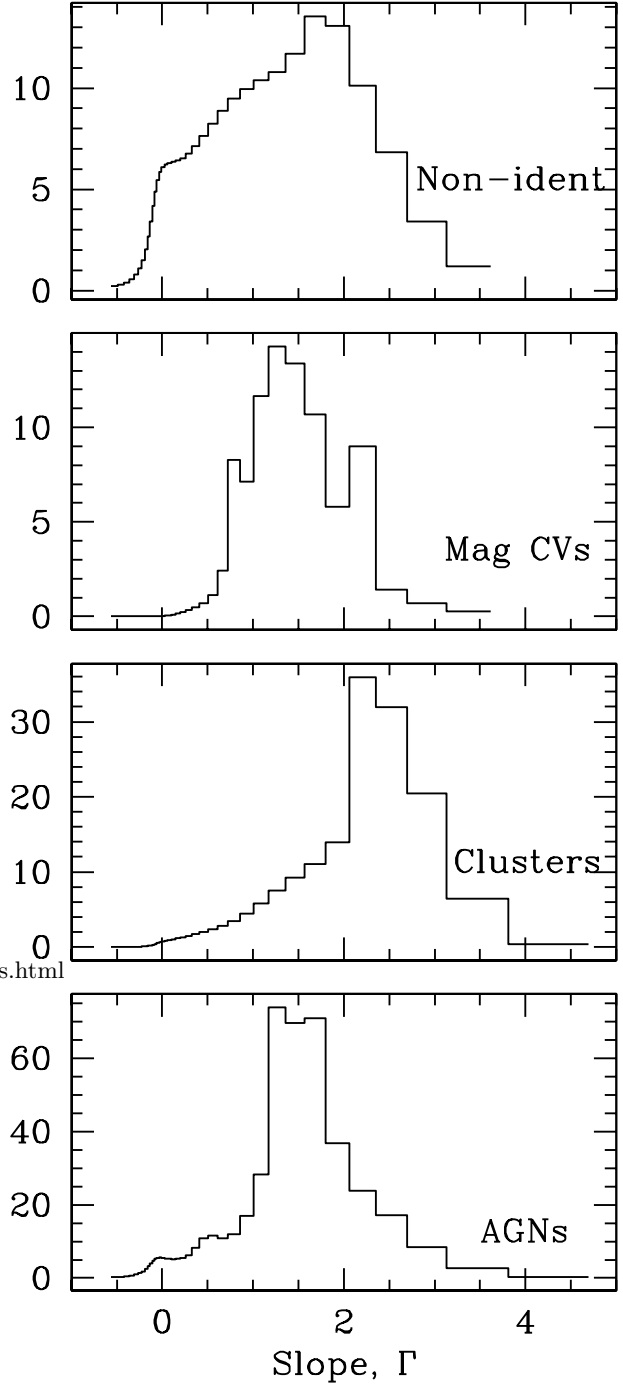


**Fig. 8.** Distribution of spectral slopes of X-ray sources detected in our survey grouped according to their astrophysical type. The contribution of each source to the corresponding diagram was computed assuming that its 8-20 keV/3-8 keV hardness ratio is described by a Gaussian distribution with the parameters determined by the values and uncertainty of the measured count rates.

**Table 2.** Catalog of sources detected in the RXTE all-sky slew survey

Name	<i>l</i>	<i>b</i>	Err(')	$F_1$	$dF_1$	$F_2$	$dF_2$	$\Gamma$	$d\Gamma$	Common name	Class1	Class2	z	R
XSS J00050-6904	309.02	-47.49	47	0.48	0.03	0.22	0.04	1.98	0.36	MRK 335	A	NLS1	0.025	1
XSS J00064+2020	108.84	-41.30	47	0.90	0.09	0.41	0.12	1.97	0.49	GRB 980203	O			
XSS J00204-1856	80.29	-79.14	47	0.31	0.03	0.08	0.04	>2.5		CGCG 535-012	A	S1	0.048	2
XSS J00368+4557	120.27	-16.83	30	0.26	0.05	0.18	0.06	1.29	0.73	A2811	C		0.11	
XSS J00411-2839	358.25	-87.26	60	0.41	0.05	-0.09	0.07	>2.2		A85	C		0.052	
XSS J00421-0916	115.47	-72.00	19	4.67	0.65	1.02	0.74	>2.2		M31	G		0.00	
XSS J00425+4102	121.12	-21.79	12	2.69	0.22	0.62	0.22	2.93	0.49	MRK 348	A	S2	0.015	
XSS J00485+3203	122.21	-30.80	38	0.71	0.04	0.82	0.04	0.50	0.13	1RXS J005528.0+461143				
XSS J00564+4548	123.85	-17.05	38	0.71	0.04	0.37	0.04	1.77	0.23	TON S180	A	NLS1	0.062	1
XSS J00569-2218	137.78	-85.02	38	0.32	0.01	0.07	0.02	2.97	0.47		G		0.00	
XSS J00595-7303	302.11	-44.06	60	6.81	0.04	6.48	0.05	0.80	0.02	SMC				
XSS J01023-4731	297.67	-69.48	60	0.39	0.07	0.33	0.11	1.02	0.66	1H 0102-469				
XSS J01078-4543	294.04	-71.11	60	0.44	0.07	0.02	0.08	>2		A2877	C		0.024	
XSS J01153-7318	300.55	-43.70	5	27.42	0.11	27.02	0.12	0.74	0.01	SMC X-1	L	XB		
XSS J01232-3502	264.20	-79.56	29	1.61	0.14	1.00	0.16	1.49	0.32	NGC 526A	A	S2	0.019	3
XSS J01236-5854	295.13	-57.73	7	1.25	0.02	0.67	0.02	1.74	0.07	Fairall 9	A	S1	0.046	
XSS J02074+1519	148.68	-43.71	60	0.33	0.18	0.19	0.21	>-0.4		TT Ari	L	NL		
XSS J02087-7418	296.03	-41.77	60	0.57	0.08	0.49	0.11	0.95	0.45					
XSS J02151-0033	163.49	-56.69	60	1.95	0.10	1.07	0.13	1.70	0.23	MRK 590	A	S1	0.027	
XSS J02284+1849	152.67	-38.38	60	1.17	0.26	0.80	0.35	>0.3		TEX 0222+185	A	Q	2.7	
XSS J02290-6931	291.07	-45.29	60	0.51	0.09	0.21	0.12	>1.5		1RXS J023052.9-684203	L	P		
XSS J02360-5234	272.61	-57.95	60	1.21	0.19	0.25	0.24	>1.9		ESO 198-G024	A	S1	0.045	
XSS J02445-0000	172.65	-51.61	60	0.67	0.16	0.11	0.18	>1.2		NGC 1068	A	S2	0.038	
XSS J02544+4133	146.34	-15.66	9	5.12	0.24	0.74	0.23	3.48	0.41	AWM 7	C		0.017	
XSS J02569+1931	159.39	-34.31	38	1.16	0.08	1.02	0.10	0.92	0.21	XY Ari	L	IP		
XSS J03008+4429	145.94	-12.51	9	2.08	0.29	0.83	0.35	2.20	0.68	CIZA J0300.7+4427	C		0.030	
XSS J03089+4101	149.07	-14.76	21	4.78	0.21	1.32	0.26	2.70	0.27	Beta Per	L	S		
XSS J03198+4128	150.61	-13.28	5	53.80	0.52	17.82	0.35	2.46	0.04	Perseus cluster	C		0.018	
XSS J03247+2836	159.26	-23.23	8	1.15	0.22	0.06	0.23	>1.8		UX Ari	L	RS CVn		
XSS J03385+0029	185.36	-41.28	12	1.08	0.11	0.11	0.11	>2.8		V711 Tau	L	RS CVn		
XSS J03389+1005	176.21	-34.93	12	2.69	0.28	0.63	0.29	2.9	0.65	2A 0335+096	C		0.035	
XSS J03429-5400	265.57	-48.77	60	1.17	0.21	0.12	0.13	>2.6		A3158	C		0.059	
XSS J03502-7417	289.02	-37.60	60	0.53	0.08	0.26	0.10	1.88	0.73	A3186	C		0.13	
XSS J03505-6846	283.24	-40.82	60	0.66	0.13	0.16	0.16	>1.5		1RXS J035257.7-683120	C		0.087	4
XSS J03558+3059	163.18	-17.10	5	13.03	0.09	5.90	0.06	2.00	0.02	X Per	L	XB		
XSS J04127+1029	182.30	-28.39	13	4.13	0.61	1.02	0.73	>2.1		A478	C		0.090	
XSS J04182+0056	192.19	-32.95	60	0.88	0.16	0.21	0.18	>1.7		1H 0414+009	A	BL	0.29	
XSS J04268-0847	203.68	-36.04	60	0.84	0.19	0.16	0.28	>0.9		EXO 0422-086	C		0.039	
XSS J04273-5749	267.71	-41.65	60	0.80	0.15	0.39	0.19	>1.8		1H 0419-577	A	S1	0.10	

**Table 2 –** continued

Name	<i>l</i>	<i>b</i>	Err(')	<i>F</i> <sub>1</sub>	d <i>F</i> <sub>1</sub>	<i>F</i> <sub>2</sub>	d <i>F</i> <sub>2</sub>	$\Gamma$	d $\Gamma$	Common name	Class1	Class2	z	R
XSS J04309-6123	272.07	-40.20	8	3.74	0.19	1.10	0.19	2.61	0.25	A3266	C		0.059	
XSS J04331+0520	190.39	-27.40	6	2.94	0.04	1.74	0.04	1.58	0.05	3C 120	A	BLRG	0.033	
XSS J04335-1316	209.59	-36.51	7	3.74	0.11	0.92	0.09	2.85	0.15	A496	C		0.033	
XSS J04562-7540	287.90	-33.21	47	0.98	0.06	0.28	0.07	2.65	0.38	ESO 033-G002	A	S2	0.018	
										YY Men	L	S		
										V1062 Tau	L	IP		
XSS J05019+2444	178.02	-10.41	9	1.72	0.15	1.18	0.18	1.34	0.30					
XSS J05054-2348	224.86	-33.19	47	0.69	0.19	0.92	0.23	0.31	0.51					
XSS J05103+1640	185.91	-13.48	60	2.08	0.19	1.18	0.23	1.65	0.36	IRAS 05078+1626	A	S1	0.018	
XSS J05150-3955	244.40	-34.83	6	6.44	0.07	2.84	0.07	2.04	0.05	4U 0513-40	L	XB		
XSS J05162-0008	201.69	-21.11	6	2.14	0.03	1.10	0.03	1.81	0.06	AKN 120	A	S1	0.033	
XSS J05168+0636	195.58	-17.59	60	0.75	0.14	0.28	0.16	>1.7		A539	C		0.029	
XSS J05178-6946	280.59	-33.36	60	1.58	0.05	0.36	0.06	2.92	0.23	1RXS J051351.2-695145	L	XB		5
XSS J05188+1823	185.61	-10.84	60	0.60	0.14	0.43	0.17	1.27	0.84					
XSS J05204-7158	283.12	-32.68	5	26.18	0.11	6.89	0.08	2.76	0.02	LMC X-2	L	XB		
XSS J05220-4603	251.96	-34.27	60	0.88	0.08	0.53	0.11	1.55	0.39	Pic A	A	BLRG	0.035	
XSS J05295-3252	236.85	-30.58	8	2.91	0.18	2.24	0.21	1.14	0.20	TV Col	L	IP		
XSS J05316+1320	191.62	-10.97	60	0.59	0.12	0.25	0.15	>1.4		PKS 0528+134	A	BL	2.1	
XSS J05329-6616	276.22	-32.52	5	5.32	0.05	6.32	0.06	0.46	0.02	LMC X-4	L	XB		
XSS J05351-0519	208.92	-19.38	7	4.82	0.18	1.08	0.18	2.96	0.23	Orion Nebula	L			
XSS J05385-5809	266.56	-32.28	60	0.70	0.12	-0.02	0.14	>1.8		TW Pic	L	NL		
XSS J05398-6404	273.56	-31.98	5	13.77	0.06	2.09	0.04	3.43	0.03	LMC X-3	L	XB		
XSS J05421-0225	207.07	-16.50	60	0.82	0.09	0.06	0.11	>2.5		Zeta Ori	L	S		
XSS J05423-7005	280.58	-31.24	21	18.19	0.06	2.40	0.04	3.60	0.03	LMC X-1	L	XB		
XSS J05432-4116	247.03	-29.78	38	0.80	0.06	0.42	0.08	1.76	0.36	TX Col	L	IP		
XSS J05450+6049	151.99	15.9	47	0.96	0.06	0.53	0.07	1.69	0.27	BY Cam	L	P		
XSS J05510-3226	237.77	-26.11	60	1.49	0.19	0.62	0.25	2.13	0.66	PKS 0548-32	A	BL	0.069	
XSS J05518-0733	212.97	-16.67	9	2.28	0.11	1.65	0.13	1.25	0.16	NGC 2110	A	S2	0.0076	
XSS J05552+4617	165.90	10.39	11	2.36	0.27	0.88	0.31	2.30	0.55	MCG +8-11-11	A	S1	0.020	
XSS J05585-3831	244.76	-26.31	10	2.33	0.34	0.76	0.38	>2.2		EXO 055625-3838.6	A	BL		
										EXO 055620-3820.2	A	S1	0.034	
XSS J06007+5346	159.50	14.62	60	1.14	0.21	0.61	0.24	1.75	0.72	V405 Aur	L	IP		
										CIZA J0602.0+5315	C		0.051	
XSS J06014-5044	258.32	-28.36	60	0.75	0.15	0.22	0.18	>1.5		PKS 0558-504	A	NLS1	0.14	
XSS J06132+4755	165.82	13.86	47	0.75	0.14	0.36	0.17	>1.8		SS Aur	L	DN		
XSS J06171+7102	143.33	22.83	34	0.36	0.07	0.67	0.09	0.00	0.22	MRK 3	A	S2	0.014	
XSS J06283-5402	262.82	-24.94	60	2.21	0.18	0.96	0.20	2.06	0.35	A3391	C		0.051	
										A3395	C		0.051	
XSS J07215+5545	161.40	26.25	13	1.10	0.10	0.24	0.14	>2.6		A576	C		0.038	
XSS J07434+4945	168.68	28.52	38	1.32	0.12	0.75	0.17	1.64	0.40	MRK 79	A	S1	0.022	
XSS J07480-6746	279.97	-19.86	5	9.41	0.05	7.09	0.05	1.18	0.02	EXO 0748-676	L	XB		
XSS J07514+1442	206.11	19.78	8	1.37	0.07	0.93	0.08	1.35	0.19	PQ Gem	L	IP		
XSS J07550+2152	199.35	23.34	10	0.84	0.05	0.31	0.07	2.29	0.35	U Gem	L	DN		
XSS J08010+6241	153.94	31.82	47	1.14	0.23	0.80	0.29	1.30	0.72	HT Cam	L	IP		
XSS J08117+7600	138.31	31.09	30	0.64	0.05	0.30	0.07	1.95	0.39	PG 0804+761	A	S1	0.10	

**Table 2 – continued**

Name	<i>l</i>	<i>b</i>	Err(')	<i>F</i> <sub>1</sub>	d <i>F</i> <sub>1</sub>	<i>F</i> <sub>2</sub>	d <i>F</i> <sub>2</sub>	$\Gamma$	d $\Gamma$	Common name	Class1	Class2	z	R
XSS J08142+6231	154.03	33.35	30	0.92	0.04	0.34	0.05	2.30	0.26	SU Uma	L	DN		
XSS J08165-0739	229.95	15.03	12	2.76	0.31	0.80	0.34	2.63	0.63	A644	C		0.071	
XSS J08300+7313	141.13	32.93	47	0.25	0.09	0.30	0.12	>0.3		Z Cam	L	DN		
XSS J08418+7052	143.54	34.46	7	1.63	0.04	1.27	0.05	1.13	0.08	S5 0836+71	A	BL	2.2	
XSS J09086-0939	239.24	24.69	7	6.12	0.15	2.40	0.13	2.22	0.09	A754	C		0.054	
XSS J09178-1208	242.93	25.02	13	1.44	0.17	0.03	0.19	>2.5		Hydra A	C		0.052	
XSS J09204+1608	214.26	40.11	60	1.06	0.22	0.79	0.28	1.19	0.71	MRK 704	A	S1	0.029	
XSS J09261+5204	165.25	44.55	60	1.17	0.10	0.54	0.13	1.98	0.42	MRK 110	A	NLS1	0.036	1
XSS J09263-3153	260.01	13.39	60	4.54	0.65	0.22	0.40	>3		4U 0923-31	L?			
XSS J09476-3100	262.77	17.18	6	6.46	0.12	3.91	0.11	1.55	0.06	MCG -5-23-16	A	S2	0.0083	
XSS J09558+6917	141.82	40.79	30	2.33	0.12	0.81	0.13	2.38	0.25	NGC 3031	A	LLAGN	0.00	
										M82	G		0.00	
XSS J10060-7600	293.34	-16.31	60	0.32	0.08	0.11	0.09	>1.1		CIZA J0957.2-7554	C			
XSS J10220+4908	165.23	53.87	60	0.47	0.10	0.27	0.17	>0.7		A990	C		0.14	
										A980	C		0.16	
XSS J10231+1950	216.96	55.35	6	2.10	0.02	1.37	0.03	1.42	0.05	NGC 3227	A	S1	0.0038	
XSS J10376-2732	269.80	26.59	30	2.80	0.13	0.50	0.16	3.23	0.41	A1060	C		0.013	
XSS J11045+3808	179.97	65.06	5	8.99	0.04	3.03	0.03	2.43	0.02	MRK 421	A	BL	0.031	
XSS J11047-2341	273.58	33.03	47	1.49	0.34	0.53	0.35	>0.3		4U 1057-21	A	BL	0.19	
XSS J11067+7234	133.24	42.40	5	3.21	0.01	1.90	0.01	1.57	0.02	NGC 3516	A	S1	0.0088	
XSS J11094-7650	297.10	-15.13	60	0.50	0.08	0.07	0.10	>1.8		Cha 1 cloud	L			6
XSS J11170+4110	170.91	66.07	60	0.35	0.06	0.18	0.07	1.80	0.78	CSO 1159	A	S1	0.095	
										PG 1115+407	A	S1	0.15	
XSS J11178+4758	157.84	62.31	5	23.70	0.16	15.93	0.11	1.37	0.02	XTE 1118+48	L	XB		
XSS J11349+6944	132.32	45.96	60	0.42	0.06	-0.05	0.07	>1.8		MRK 180	A	BL	0.045	
XSS J11393-3745	287.52	22.95	5	4.90	0.04	2.93	0.05	1.57	0.04	NGC 3783	A	S1	0.0097	
XSS J11406+4617	154.40	66.27	60	0.34	0.08	0.20	0.10	>1		A1361	C		0.12	
XSS J11417+5910	138.76	55.76	16	0.41	0.06	0.20	0.08	1.89	0.69	SBS 1136+594	A	S1	0.060	
XSS J11444+1952	234.64	73.03	14	2.76	0.14	0.57	0.14	3.05	0.32	A1367	C		0.022	
XSS J11474+7143	129.88	44.52	7	1.60	0.12	1.00	0.14	1.48	0.27	DO Dra	L	IP		
XSS J11559-2637	287.84	34.61	60	1.10	0.02	0.48	0.02	2.05	0.10	GRB 990506	O			
XSS J11570+5514	138.56	60.19	60	0.48	0.07	0.07	0.09	>1.9		NGC 3998	A	LLAGN	0.0035	7
XSS J12011+2920	198.65	78.71	60	0.53	0.09	0.30	0.12	1.65	0.75	RX J1201.5+2932	A	S1	0.13	
										4C +29.45	A	BL	0.73	
										RX J1203.7+2836	A	Q	0.37	
XSS J12032+4424	149.04	70.18	21	1.49	0.02	0.73	0.02	1.88	0.07	NGC 4051	A	NLS1	0.0023	1
XSS J12106+3927	154.87	75.02	5	9.46	0.04	6.82	0.05	1.25	0.02	NGC 4151	A	S1	0.0033	
XSS J12164+1427	268.42	74.94	60	0.59	0.08	0.23	0.09	2.22	0.66	PG 1211+143	A	NLS1	0.081	1
XSS J12190+3003	188.70	82.30	47	1.77	0.12	0.61	0.13	2.39	0.33	TON 0605	A	BL	0.24	
										NGC 4253	A	NLS1	0.013	
										FBQS J1221+3010	A	BL	0.18	
XSS J12190+4715	138.34	68.89	21	0.81	0.02	0.51	0.02	1.48	0.10	NGC 4258	A	S2	0.0015	
XSS J12201+0329	284.01	65.20	25	1.07	0.17	0.45	0.21	>2		ZwCl 1215	C		0.075	
XSS J12206+7509	125.57	41.81	60	0.37	0.06	0.14	0.07	>1.8		MRK 205	A	S1	0.070	
XSS J12260+1248	279.16	74.49	30	4.33	0.10	2.61	0.10	1.55	0.08	NGC 4388	A	S2	0.0084	
XSS J12270-4859	298.81	13.67	9	1.32	0.13	0.67	0.15	1.82	0.41	1RXS J122758.8-485343				
XSS J12288+0200	289.81	64.29	6	6.77	0.05	4.28	0.04	1.47	0.03	3C 273	A	BL	0.16	

**Table 2** – continued

Name	<i>l</i>	<i>b</i>	Err(')	<i>F</i> <sub>1</sub>	d <i>F</i> <sub>1</sub>	<i>F</i> <sub>2</sub>	d <i>F</i> <sub>2</sub>	$\Gamma$	d $\Gamma$	Common name	Class1	Class2	<i>z</i>	<i>R</i>
XSS J12303-4232	298.78	20.16	60	0.48	0.09	0.28	0.10	1.57	0.72	1RXS J123212.3-421745=IRAS F12295-4201				
XSS J12309+1223	283.89	74.49	6	16.05	0.15	2.30	0.08	3.49	0.05	M87/Virgo	C		0.0044	
XSS J12312+0833	287.59	70.82	60	0.45	0.10	0.14	0.11	>1.3		M49	G		0.0033	
XSS J12351-3948	299.54	22.95	60	0.29	0.11	0.57	0.13	<0.6		NGC 4507	A	S2	0.012	
XSS J12389-1614	298.56	46.53	60	0.93	0.11	0.51	0.12	1.71	0.46					
XSS J12392-3820	300.30	24.46	60	0.62	0.07	0.23	0.08	2.26	0.54	V1025 Cen	L	IP		
XSS J12408-0516	298.00	57.50	60	1.05	0.16	0.61	0.18	1.59	0.58	NGC 4593	A	S1	0.0090	
XSS J12490-4120	302.44	21.53	6	8.54	0.12	1.92	0.09	2.96	0.07	Centaurus cluster	C		0.010	
XSS J12529-2911	303.32	33.68	6	6.22	0.12	2.49	0.09	2.19	0.07	EX Hya	L	IP		
XSS J12553-2633	304.00	36.30	60	0.46	0.08	0.20	0.10	>1.6		CTS M12.22	A	S1	0.058	
XSS J12565-0537	305.27	57.21	26	0.76	0.02	0.48	0.02	1.47	0.11	3C 279	A	BL	0.54	
XSS J12572-3049	304.41	32.03	60	1.02	0.11	0.20	0.13	>2.6		A3532	C		0.054	
										A3530	C		0.054	
XSS J12575-1727	304.99	45.39	9	1.97	0.08	0.54	0.09	2.69	0.23	A1644	C		0.047	
XSS J12587-0408	306.44	58.67	60	1.67	0.07	0.60	0.07	2.34	0.20	A1651	C		0.085	
XSS J12595-0114	307.19	61.56	60	0.78	0.13	0.16	0.10	>2.4		A1650	C		0.085	
XSS J12596+2759	58.86	87.98	9	22.21	0.09	8.68	0.07	2.22	0.02	Coma cluster	C		0.023	
XSS J13021-7638	303.56	-13.77	60	0.40	0.08	0.15	0.09	>1.5		Cha 2 cloud	L		6	
XSS J13073-4926	305.58	13.35	60	0.30	0.05	0.30	0.06	0.72	0.42	NGC 4945	A	S2	0.0019	
XSS J13085-4018	306.45	22.44	60	0.31	0.11	0.46	0.14	0.19	0.65	ESO 323-G077	A	S1	0.015	8
XSS J13124-0125	313.80	61.00	60	0.81	0.12	0.24	0.14	>2.1		A1689	C		0.18	
XSS J13166-2453	310.15	37.62	60	0.20	0.06	0.14	0.07	>0.6		1RXS J131423.6-251521	C		0.25	
XSS J13253-4302	309.49	19.39	5	13.00	0.17	9.51	0.17	1.23	0.04	Cen A	A	NLRG	0.0018	
XSS J13276-2711	312.75	34.99	60	1.44	0.07	0.41	0.08	2.63	0.27	A1736	C		0.046	
XSS J13284-3134	312.09	30.64	5	5.14	0.05	1.56	0.03	2.57	0.04	A3558	C		0.048	
XSS J13312-2502	314.22	36.96	60	0.25	0.06	0.15	0.07	>1.3		ESO 509-G038	A	S1	0.026	
XSS J13352-3143	313.72	30.22	60	1.06	0.04	0.26	0.05	2.84	0.28	A3562	C		0.050	
XSS J13354-3414	313.20	27.74	5	3.08	0.02	1.65	0.02	1.74	0.04	MCG -6-30-15	A	S1	0.0077	
XSS J13355+3714	83.03	76.25	60	3.70	0.50	0.42	0.39	>2.8		BH CVn	L	RS CVn		
XSS J13420-1432	320.90	46.55	60	0.47	0.08	0.26	0.09	1.71	0.67	NPM1G -14.0512	A	NLS1	0.042	1
XSS J13473-3252	316.28	28.54	5	6.79	0.09	2.20	0.09	2.49	0.07	A3571	C		0.040	
XSS J13486+2642	34.27	77.25	17	3.53	0.24	0.78	0.25	2.97	0.43	A1795	C		0.062	
XSS J13492-3020	317.47	30.89	5	7.29	0.07	4.20	0.08	1.62	0.04	IC 4329A	A	S1	0.016	
XSS J13530+6916	115.03	46.89	47	2.13	0.06	1.04	0.07	1.89	0.13	MRK 279	A	S1	0.031	
XSS J13563-7342	307.51	-11.41	17	0.54	0.10	0.24	0.12	>1.6		1H 1342-733				
XSS J13578-4214	315.85	18.96	60	0.38	0.08	0.29	0.10	1.18	0.71	PKS 1355-41	A	RLQ	0.31	9
XSS J13588-4738	314.53	13.69	47	2.04	0.15	0.61	0.16	2.59	0.39	CIZA J1358.9-4750	C			
XSS J13598+0319	340.37	61.11	60	0.56	0.12	0.41	0.17	1.22	0.83	A1835	C		0.25	
XSS J14044-3326	320.00	27.00	60	0.32	0.07	0.07	0.08	>1.4		NGC 5419	G		0.014	
XSS J14080-5042	315.12	10.34	47	1.52	0.11	0.53	0.12	2.37	0.35	CIZA J1407.8-5100	C		0.097	
XSS J14100-4500	317.23	15.66	60	0.85	0.08	0.52	0.09	1.53	0.36	V834 Cen	L	P		

Table 2 – continued

Name	<i>l</i>	<i>b</i>	Err(')	<i>F</i> <sub>1</sub>	d <i>F</i> <sub>1</sub>	<i>F</i> <sub>2</sub>	d <i>F</i> <sub>2</sub>	$\Gamma$	d $\Gamma$	Common name	Class1	Class2	z	R					
XSS J14101-2936	322.74	30.22	60	0.25	0.07	0.31	0.09	0.42	0.60	CIZA J1410.4-4246 NGC 5506 1RXS J141650.6-115845=LCRS B141408.4-114506 PKS 1416-49 NGC 5548 ESO 511-G030 A1904 ZwCl 1420.2+4952 H 1419+480	C A G(A?) A A A C C A	S2 0.0062 0.099 RG S1 S1 0.071 0.071 S1	0.049 0.092 0.099 0.092 0.017 0.022 0.071 0.071 0.072	10					
XSS J14102-4221	318.14	18.17	47	1.00	0.16	0.51	0.19	1.81	0.68										
XSS J14132-0311	339.16	53.82	5	6.90	0.03	3.71	0.02	1.74	0.02										
XSS J14138-4022	319.49	19.83	47	0.52	0.09	0.24	0.11	1.95	0.79										
XSS J14170-1133	333.97	46.08	60	0.57	0.09	0.22	0.13	>1.6	0.03										
XSS J14176-4910	317.10	11.30	60	0.52	0.10	0.28	0.13	>1.7											
XSS J14181+2514	32.26	70.48	6	3.58	0.02	2.03	0.02	1.65	NGC 5548	A	S1	0.017							
XSS J14194-2606	326.51	32.70	60	1.10	0.09	0.70	0.09	1.46	ESO 511-G030	A	S1	0.022							
XSS J14199+4837	90.28	62.51	60	0.32	0.05	0.09	0.06	>1.8	A1904	C		0.071							
									ZwCl 1420.2+4952	C		0.071							
									H 1419+480	A	S1	0.072							
XSS J14239-3800	322.35	21.35	60	0.77	0.12	0.38	0.14	1.84	0.66	1RXS J142149.8-380901									
XSS J14241-4803	318.54	11.98	60	0.33	0.04	0.05	0.05	>2.2	1RXS J142148.7-480420										
XSS J14244+3753	67.66	67.71	20	1.13	0.19	0.30	0.23	>1.8	A1914	C		0.17							
XSS J14278+4240	77.65	65.00	47	1.17	0.08	0.54	0.11	1.95	0.35	H 1426+428	A	BL	0.13						
XSS J14353-3557	325.47	22.32	60	0.34	0.07	0.20	0.09	>1.4											
XSS J14408-3815	325.47	19.77	60	0.73	0.07	0.28	0.08	2.26	0.47	1RXS J144037.4-384658									
XSS J14495-4005	326.19	17.38	47	0.42	0.04	0.18	0.05	2.06	0.50										
XSS J14527-2414	335.37	30.87	47	0.75	0.05	0.21	0.06	2.68	0.42	1RXS J145017.6-242558	L	S		0.32					
XSS J14562-3735	328.66	18.96	60	0.41	0.05	0.30	0.06	1.25	0.42	PKS 1451-375	A	RLQ							
										CIZA J1456.2-3826	C								
XSS J15031-4149	327.68	14.61	60	2.00	0.06	0.46	0.06	2.91	0.17	SN1006	L		0.036	0.045					
XSS J15042+1046	11.75	54.76	60	0.95	0.14	0.32	0.16	>2.1	MRK 841	A	S1								
XSS J15076-4257	327.82	13.23	60	0.73	0.05	0.24	0.05	2.47	0.36										
XSS J15103-2042	341.63	31.52	60	0.61	0.10	0.07	0.12	>1.5	IRAS 15091-2107	A	NLS1	0.045	0.077						
XSS J15110+0541	6.43	50.49	8	4.32	0.17	1.53	0.20	2.36	0.20	A2029	C								
XSS J15128-0858	351.39	40.22	38	0.59	0.03	0.50	0.03	0.96	0.16	PKS 1510-08	A	BL		0.36					
XSS J15145-4551	327.36	10.11	60	1.27	0.17	0.00	0.20	>2.2	CIZA J1514.6-4558	C		0.058							
XSS J15153-3802	331.80	16.64	60	0.24	0.05	0.09	0.06	>1.3											
XSS J15179-3559	333.44	18.05	60	0.12	0.05	0.12	0.06	>0.3											
XSS J15228+0829	12.61	49.67	60	1.49	0.17	0.20	0.19	>2.6	A2063	C		0.035	0.045						
										MKW 3S	C			0.045					
XSS J15348+5750	91.50	48.10	60	0.68	0.07	0.37	0.09	1.71	0.44	MRK 290	A	S1	0.030	0.025					
XSS J15360-4118	333.24	11.68	60	0.27	0.06	0.17	0.07	1.44	0.83										
XSS J15478-1350	354.77	30.76	60	1.06	0.14	0.39	0.17	2.29	0.69	NGC 5995	A	S2	0.025						
XSS J15582+2716	44.28	48.71	7	4.56	0.23	2.08	0.26	1.99	0.21	A2142	C		0.089	0.15					
XSS J16019-7548	313.86	-17.16	10	1.26	0.12	0.18	0.11	>3.1	CIZA J1601.7-7544	C									
XSS J16020+1607	29.07	44.63	38	2.00	0.23	0.46	0.25	>2.6	A2147	C		0.035							
										Gin 463	A		0.11						
XSS J16049-7302	315.99	-15.29	60	0.40	0.09	0.30	0.10	1.20	0.73	GRB 971209 1RXS J161519.2-093618, 1H 1613-097 A2163 V893 Sco	O C C L	DN XB	0.20	0.02					
XSS J16058+6014	92.06	43.46	60	0.27	0.02	0.00	0.03	>2.8											
XSS J16151-0943	3.40	28.41	60	0.56	0.14	0.25	0.16	>1.1											
XSS J16159-0604	6.86	30.46	11	1.82	0.19	1.10	0.22	1.55	0.38	A2163									
XSS J16167-2817	348.55	15.88	38	2.38	0.16	0.96	0.18	2.18	0.31	V893 Sco									
XSS J16204-1536	359.19	23.70	13	13149.73	36.32	3070.94	40.38	2.91	0.02	Sco X-1	L	XB							

Table 2 – continued

Name	<i>l</i>	<i>b</i>	Err(')	$F_1$	$dF_1$	$F_2$	$dF_2$	$\Gamma$	$d\Gamma$	Common name	Class1	Class2	z	R
XSS J16253+5201	80.16	43.25	60	0.25	0.07	0.20	0.08	>0.8		SBS 1624+514	A	BLRG	0.18	
XSS J16265-3303	346.47	11.07	60	1.66	0.14	0.55	0.16	2.46	0.44	CIZA J1626.3-3329	C		0.11	
XSS J16265-2931	349.14	13.46	60	0.51	0.07	0.23	0.09	1.98	0.66	CIZA J1627.9-2952	C			
XSS J16271-2423	353.18	16.79	60	1.81	0.13	0.35	0.15	3.13	0.60	Rho Oph cloud	L			
XSS J16273+3935	62.97	43.94	9	3.98	0.23	0.75	0.24	3.17	0.42	A2199	C		0.030	
XSS J16323-6730	321.74	-13.13	5	10.20	0.09	10.16	0.09	0.72	0.03	4U 1627-673	L	XB		
XSS J16345-7506	315.85	-18.18	60	1.02	0.11	0.39	0.13	2.25	0.55	A3628	C		0.15	
XSS J16384-6424	324.56	-11.56	6	7.95	0.14	3.30	0.14	2.14	0.08	Triangulum Australis	C		0.051	
XSS J16385+4711	73.28	41.74	60	0.70	0.08	0.32	0.09	1.97	0.51	A2219	C		0.23	
XSS J16431-7310	317.82	-17.44	60	0.51	0.09	0.26	0.12	1.77	0.81	CIZA J1645.4-7334	C		0.069	
XSS J16536+3951	63.72	38.90	5	9.46	0.04	5.19	0.05	1.70	0.02	MRK 501	A	BL	0.033	
XSS J16537-1905	1.50	15.30	60	0.82	0.15	0.58	0.17	1.29	0.60	1H 1652-180				
XSS J16581+3522	58.20	37.46	5	8.06	0.06	11.52	0.09	0.23	0.02	Her X-1	L	XB		
XSS J17046-0110	18.90	22.98	60	1.27	0.18	0.31	0.21	>2.2		UGC 10683	A	S1	0.031	
										ZwCl 1703.8-0129	C			
										1RXS J170211.0-010118				
XSS J17050+7838	110.99	31.70	7	3.56	0.13	1.37	0.13	2.25	0.16	A2256	C		0.056	
XSS J17070+2354	45.12	32.86	5	6.34	0.18	6.84	0.22	0.60	0.07	4U 1700+24	L	XB		
XSS J17115+6426	94.41	34.98	60	0.66	0.11	0.13	0.13	>1.9		A2255	C		0.081	
XSS J17169-6232	328.72	-13.89	60	0.44	0.11	0.51	0.14	0.50	0.58	NGC 6300	A	S2	0.0037	
XSS J17214+3239	56.12	32.20	60	0.62	0.12	0.31	0.14	>1.7		A2261	C		0.22	
XSS J17214+2653	49.61	30.65	60	0.78	0.15	0.32	0.17	>1.7		1RXS J172009.3+263727	C		0.16	
										A2259	C		0.16	
XSS J17223-7301	319.60	-19.73	60	0.38	0.08	0.14	0.09	>1.4		1RXS J171850.0-732527				
XSS J17272+5025	77.30	33.71	60	0.60	0.12	0.35	0.15	1.60	0.82	I Zw 187	A	BL	0.055	
XSS J17276-1359	10.54	11.46	60	0.58	0.05	0.16	0.08	2.65	0.69	PDS 456	A	RQQ	0.18	
XSS J17309-0552	18.11	14.93	60	0.67	0.15	0.36	0.18	>1.3		1RXS J173021.5-055933, 1H 1726-058				
XSS J17413-5354	338.00	-12.15	60	0.43	0.08	0.17	0.10	>1.5						
XSS J17413+1851	42.84	23.62	47	1.56	0.18	0.65	0.25	2.12	0.62	4C +18.51	A	RLQ	0.19	9
XSS J17459+1115	35.83	19.56	60	0.26	0.22	0.13	0.27	< 4.7		1RXS J174527.8+110837=IRAS F17431+1109				
XSS J17576-4534	346.73	-10.42	60	0.49	0.09	0.30	0.12	1.50	0.79					
XSS J17597+0821	34.62	15.26	60	1.33	0.10	0.74	0.12	1.68	0.30	V2301 Oph	L	P		
XSS J18036+0100	28.32	11.08	60	0.67	0.12	0.33	0.14	1.89	0.75	CIZA J1804.1+0042	C		0.088	
XSS J18076+5937	88.50	28.60	60	0.11	0.02	-0.03	0.03	>1		GRB 970828	O			
XSS J18080+0622	33.72	12.53	35	1.12	0.21	0.63	0.26	1.64	0.77	V426 Oph	L	DN		
XSS J18164+5004	78.08	25.88	7	3.21	0.12	2.38	0.14	1.21	0.13	AM Her	L	P		
XSS J18196+6454	94.60	27.71	60	0.90	0.13	0.21	0.16	>2.1		H 1821+643	A	RQQ	0.30	
XSS J18236-5616	338.49	-18.62	60	0.32	0.09	0.50	0.12	0.13	0.43					
XSS J18239+3041	58.43	18.91	60	0.87	0.11	0.27	0.12	2.53	0.67	CIZA J1824.1+3029	C		0.065	
										CIZA J1825.3+3026	C			
XSS J18258-3700	356.94	-11.26	5	33.44	0.23	28.04	0.23	1.00	0.02	4U 1822-371	L	XB		
XSS J18348+3238	61.23	17.47	8	2.29	0.13	1.40	0.15	1.53	0.21	3C 382	A	BLRG	0.059	
XSS J18360-3300	1.53	-11.44	5	10.74	0.04	6.35	0.03	1.58	0.02	XB 1832-330	L	XB		
XSS J18362-5918	336.04	-21.22	30	1.00	0.06	0.36	0.06	2.34	0.29	Fairall 49	A	S2	0.020	

**Table 2 – continued**

Name	<i>l</i>	<i>b</i>	Err(')	<i>F</i> <sub>1</sub>	d <i>F</i> <sub>1</sub>	<i>F</i> <sub>2</sub>	d <i>F</i> <sub>2</sub>	$\Gamma$	d $\Gamma$	Common name	Class1	Class2	z	R
XSS J18376-6511	330.00	-23.04	47	1.27	0.07	0.98	0.08	1.13	0.18	ESO 103-G035	A	S2	0.013	
XSS J18381-5653	338.60	-20.72	60	0.33	0.12	0.36	0.15	>0.3						
XSS J18408+7947	111.45	27.13	6	1.66	0.02	0.97	0.03	1.60	0.07	3C 390.3	A	BLRG	0.056	
XSS J18449-6204	333.50	-23.02	38	0.78	0.11	0.35	0.13	2.01	0.65	ESO 140-G043	A	S1	0.014	
XSS J18486-2649	8.43	-11.30	47	0.74	0.14	0.32	0.16	>1.6						
XSS J18494-7829	315.79	-26.44	47	1.15	0.09	0.58	0.11	1.83	0.35	H 1846-786	A	S1	0.074	
XSS J18553-3111	4.95	-14.42	6	6.86	0.13	5.24	0.12	1.16	0.06	V1223 Sgr	L	IP		
XSS J19052+5212	82.59	19.11	60	0.36	0.14	0.06	0.18	>0		CG Dra	L	DN		
XSS J19202-5849	337.98	-26.61	10	1.37	0.12	0.80	0.15	1.61	0.36	ESO 141-G055	A	S1	0.036	
XSS J19210+4359	75.71	13.54	6	9.57	0.13	3.74	0.13	2.22	0.06	A2319	C		0.056	
XSS J19243+5041	82.26	15.78	60	0.76	0.11	0.95	0.14	0.39	0.30	CH Cyg	L	SS		
XSS J19303-7950	314.33	-28.38	60	0.69	0.12	0.33	0.15	>1.9		1RXS J194944.6-794519				
XSS J19397-1019	29.02	-15.36	60	1.39	0.07	1.17	0.09	1.00	0.16	V1432 Aql	L	P		
										NGC 6814	A	S1	0.0052	
XSS J19412-7619	318.28	-29.23	60	0.49	0.09	-0.04	0.11	>1.6		AA Oct	L	S		
XSS J19459+4508	78.80	10.08	60	0.38	0.09	0.38	0.12	0.73	0.68					
XSS J19592+6505	97.91	17.71	6	4.11	0.10	1.11	0.12	2.72	0.15	1ES 1959+650	A	BL	0.047	
XSS J20085-4833	350.67	-32.43	5	3.80	0.07	2.66	0.07	1.31	0.06	PKS 2005-489	A	BL	0.071	
XSS J20114-5648	340.89	-33.25	8	3.91	0.16	1.39	0.18	2.36	0.20	A3667	C		0.056	
XSS J20348+2157	64.71	-10.92	60	0.73	0.16	0.49	0.20	1.38	0.81	4C +21.55	A	RG		12
XSS J20404+7521	109.11	19.76	60	1.08	0.13	0.63	0.16	1.59	0.48	4C +74.26	A	RLQ	0.10	9
XSS J20426-3225	11.19	-36.49	60	0.49	0.09	0.03	0.10	>1.7		AT Mic	L	S		
XSS J20441-1042	35.99	-29.84	7	3.12	0.10	1.68	0.10	1.73	0.12	MRK 509	A	S1	0.034	
XSS J20501-5646	340.42	-38.53	60	0.71	0.12	0.65	0.15	0.85	0.50	IC 5063	A	S2	0.011	
XSS J21128+8216	116.11	22.49	60	0.46	0.12	0.35	0.15	>1.1		S5 2116+81	A	BLRG	0.084	13
XSS J21155-5836	337.11	-41.43	47	0.44	0.08	0.31	0.09	1.26	0.63	CD Ind	L	P		
XSS J21212-0607	45.83	-35.93	5	9.93	0.19	8.67	0.25	0.94	0.06	XTE J2123-058	L	XB		
XSS J21296+1208	64.93	-27.27	5	15.90	0.16	5.36	0.11	2.43	0.04	M15/4U 2127+119	L	XB		
XSS J21310-6219	331.58	-41.98	60	0.50	0.10	0.18	0.12	>1.5		IRAS F21325-6237	A	S1	0.059	
XSS J21354-2720	20.88	-46.73	60	0.40	0.11	0.32	0.13	1.11	0.87	1RXS J213445.2-272551, 1H 2132-277				
XSS J21445+3823	87.35	-11.24	5	568.51	2.02	153.18	0.54	2.73	0.01	Cyg X-2	L	XB		
XSS J21481-3036	16.69	-49.99	60	0.72	0.13	0.80	0.15	0.56	0.40	A3814	C		0.12	
										RX J2146.6-3051	A	S1	0.076	
										PKS 2149-306	A	BL	2.35	
XSS J21583-3004	17.95	-52.11	5	5.04	0.05	2.07	0.03	2.15	0.03	PKS 2155-304	A	BL	0.12	
XSS J22013-3147	15.24	-52.90	50	1.17	0.06	0.80	0.07	1.35	0.18	NGC 7172	A	S2	0.0086	
XSS J22023+4226	92.63	-10.26	30	0.61	0.03	0.37	0.04	1.54	0.21	BL Lac	A	BL	0.069	
XSS J22082-4708	349.70	-52.42	18	1.12	0.16	0.57	0.18	1.83	0.58	NGC 7213	A	S1	0.0060	
XSS J22088-1159	46.47	-49.06	60	0.70	0.08	0.12	0.09	>2.6		A2420	C		0.085	
XSS J22129+1239	73.75	-34.66	47	1.24	0.15	0.51	0.17	2.15	0.56	RU Peg	L	DN		
										A2424	C		0.15	
XSS J22145-0959	50.18	-49.29	60	0.93	0.07	0.16	0.08	3.25	0.68	A2426	C		0.10	
										A2428	C		0.085	
XSS J22178-0822	52.95	-49.14	7	2.41	0.07	2.27	0.08	0.81	0.09	FO Aqr	L	IP		
XSS J22355-2601	27.17	-59.67	7	2.16	0.04	1.20	0.05	1.68	0.08	NGC 7314	A	S2	0.0047	

**Table 2** – continued

Name	<i>l</i>	<i>b</i>	Err(')	<i>F</i> <sub>1</sub>	d <i>F</i> <sub>1</sub>	<i>F</i> <sub>2</sub>	d <i>F</i> <sub>2</sub>	$\Gamma$	d $\Gamma$	Common name	Class1	Class2	<i>z</i>	R
XSS J22363-1230	51.03	-55.18	60	0.79	0.16	0.50	0.21	1.46	0.81	MRK 915	A	S1	0.024	
XSS J22423+2958	92.21	-25.08	38	1.13	0.02	0.35	0.02	2.53	0.12	AKN 564	A	NLS1	0.025	
XSS J22461-6410	322.67	-47.87	60	0.65	0.11	0.17	0.13	>1.8		A3921	C		0.094	
XSS J22526+1650	86.27	-37.43	43	1.96	0.04	0.83	0.05	2.09	0.10	IM Peg	L	RS CVn		
XSS J22539-1735	46.14	-61.29	10	2.10	0.11	1.36	0.12	1.43	0.18	MR 2251-178	A	RQQ	0.064	
XSS J22551-0309	68.65	-53.31	8	2.20	0.09	1.33	0.10	1.54	0.15	AO Psc	L	IP		
XSS J23033+0858	83.22	-45.39	26	1.69	0.01	0.91	0.01	1.73	0.03	NGC 7469	A	S1	0.016	
XSS J23040-0834	64.05	-58.56	60	1.61	0.08	1.06	0.11	1.41	0.20	MRK 926	A	S1	0.047	
XSS J23073+0447	80.76	-49.36	60	0.54	0.10	0.36	0.11	1.39	0.65	PG 2304+042	A	S1	0.042	
XSS J23101-2204	39.74	-66.48	60	0.67	0.15	0.30	0.18	>1.2		MS 2306.1-2236	A	BL	0.14	
										A2556	C		0.087	
XSS J23115-5922	324.10	-53.44	60	0.64	0.14	0.12	0.16	>1.4		CP Tuc	L	P		
XSS J23178-4236	347.70	-65.48	47	0.58	0.03	0.41	0.04	1.27	0.21	NGC 7582	A	S2	0.053	
XSS J23449-2826	23.98	-75.24	60	0.93	0.17	0.12	0.21	>1.6		A4038	C		0.030	
XSS J23556+2848	108.42	-32.48	47	0.71	0.08	0.05	0.08	>2.7		II Peg	L	RS CVn		
XSS J23557-3405	359.31	-76.15	47	0.71	0.11	0.11	0.15	>1.7		A4059	C		0.047	

<sup>1</sup> – Véron-Cetty et al. 2001<sup>2</sup> – Direct examination of the ROSAT all-sky survey map reveals a source coinciding with the AGN<sup>3</sup> – Véron-Cetty & Véron 2003<sup>4</sup> – or BL Lac object, Fischer et al. 1998<sup>5</sup> – located in LMC<sup>6</sup> – Alcalá et al. 1995<sup>7</sup> – Pellegrini et al. 2000<sup>8</sup> – Schmid et al. 2003, Della Ceca et al. 1990<sup>9</sup> – Brinkmann et al. 1997<sup>10</sup> – Simpson et al. 1996<sup>11</sup> – Imanishi et al. 2001<sup>12</sup> – Laurent-Muehleisen et al. 1997<sup>13</sup> – Lara et al. 1999